SEMIANNUAL PROGRESS REPORT

December 31, 1961

RESEARCH ON PHYSICAL AND CHEMICAL PRINCIPLES AFFECTING HIGH TEMPERATURE MATERIALS FOR ROCKET NOZZLES

UNION CARBIDE RESEARCH INSTITUTE
Tarrytown, New York

PARMA RESEARCH CENTER
Cleveland, Ohio

Laboratories of Union Carbide Corporation

Prepared by: Robert Lowrie
Robert Lowrie

Submitted by: R. H. Crist
R. H. Crist, Director
UC Research Institute

Project Director: Verner Schomaker
Verner Schomaker

Contract No. DA-30-069-ORD-2787
Under the Auspices of
Advanced Research Projects Agency
and
Army Rocket and Guided Missile Agency

FOREWORD

This research program is being carried out in the research laboratories of Union Carbide Corporation located at Tarrytown, New York (Union Carbide Research Institute) and at Parma, Ohio (Parma Research Center). The work is supported by the Advanced Research Projects Agency under Contract No. DA-30-069-ORD-2787 with the Army Rocket and Guided Missile Agency, Redstone Arsenal, Alabama. The report period is from July 1, 1961 to December 31, 1961.

The program at Union Carbide Research Institute is under the project direction of Dr. Verner Schomaker with Dr. R. H. Crist serving as general project coordinator and Director of the Institute. Work at the Parma Research Center is under the supervision of Dr. R. G. Breckenridge.

The scope of the program as stated in the contract is "to obtain a better understanding of the mechanisms which govern the behavior of materials in high temperature environments, to learn how to make the most effective use of available materials, and to obtain a better knowledge of optimum properties desired for new materials for particular uses. The work is expected to provide guidance for those concerned with the development of materials and the use of materials in solid-propellant engines."

TABLE OF CONTENTS

I SUMMARY

Semiquantitative screening studies of the influence upon rocket-nozzle erosion of chemical reaction between the nozzle and the exhaust have been made. A rapid test has been developed in which a simple, prismatic sample is heated in a selected atmosphere by an arc-image furnace. Thus far, a number of refractory carbides and borides, several grades of graphite, and tungsten have been exposed to CO, CO_2, H_2, H_2O, HCl, and BF_3 and to some binary mixtures of these. The CO reacted only slightly with any of these materials, H_2 reacted appreciably only with graphite, and CO_2 and H_2O oxidized all these refractory solids (with tungsten having the best resistance). Although some difficulties involving reaction with the tantalum holders may have affected the HCl and BF_3 results, graphite and tungsten were best in HCl and BF_3, and the carbides and borides were less resistant. More work on the reaction of gas mixtures, especially CO/CO_2 and H_2/H_2O, is planned, as is work with HF and possibly gaseous $AlCl_3$ and liquid Al_2O_3. The reactions will be further studied by metallographic methods, determination of changes in weight and dimensions, and establishment of the reaction products.

Quantitative measurements have been made of the reactions of hydrogen with graphite and of hydrogen with titanium carbide. Some conclusions drawn from the studies on graphite are that the rates of production of methane and acetylene at zero time are approximately first order and equal to 6.2×10^{-10} and 2.3×10^{-10} moles/cm^2 of graphite/mm Hg/sec, respectively, at 2150°C. There is a sharp break near 2050°C in the Arrhenius plot of the production rate of propane. Sublimation of C_3 molecules may be the rate-controlling step. Studies using deuterium indicate that the reaction to form acetylene may involve more than a single hydrogen molecule. Methane, unaccompanied by acetylene, was found as the main reaction product of TiC with hydrogen, in contrast to the reaction of graphite with hydrogen. Future plans include use of the techniques developed in work with hydrogen for determination of the gaseous products of reactions of a variety of rocket-exhaust components with carbides or borides.

The vaporization of ZrB_2 has been studied with the mass spectrometer. Values of about -55 kcal/mole were obtained for the heat of formation of ZrB_2 at 25°C, and a value of 460 kcal/mole for its heat of vaporization at 25°C. Reactions were found to occur between ZrB_2 and both graphite and tungsten crucibles near 2100°C. More experiments are planned to check these results, possibly including determinations of the vapor pressure of zirconium, and hence its heat of vaporization, for use in calculation of the heat of vaporization of ZrB_2. Equipment will also be assembled for conducting gas-solid reactions either by admitting the gas to a Knudsen cell containing a carbide or boride or by impinging a molecular beam upon a refractory sample. In either case the reaction products (equilibrium or kinetic respectively) will be monitored by the mass spectrometer.

A completion report has been written on the spectra of B_2O_3 and B_2O_2 molecules trapped in argon and xenon matrices. A vibrational assignment has been made for the B_2O_3 molecule, and from this the molecular force constants have been obtained using an IBM 7090 computer. Experiments have been made with carbon vapor trapped in neon and xenon matrices for comparison with previous argon-matrix work. A red shift that increases with the size of the matrix molecule (Ne < A < Xe) is found for certain bands. Some splitting of bands that was different in different matrices was also observed. This matrix-isolation technique, demonstrated to be of general usefulness by the work on B_2O_3 and graphite, will be available for work on refractory compounds that appear promising in the chemical screening tests.

The dynamic elastic constants of monocrystalline tungsten have been determined at room temperature. The results agree excellently with those obtained with a different technique by de Klerk and Bolef. Similar determinations of the dynamic elastic constants of single crystals of ZrC and TiC are also reported. The elastic constants of a hot-pressed polycrystalline sample of TiC were also measured at room temperature. Comparison of the elastic constants of hot-pressed TiC samples with values calculated for an idealized polycrystalline material from the data on monocrystalline TiC shows that Poisson's ratio changes little with density, but that the elastic moduli decrease rapidly as porosity increases. Velocities of ultrasonic wave propagation have been measured in pyrolytic graphite at room temperature. Some

dynamic elastic constants were calculated from these data and the assumption that the basal planes of the individual crystallites are all parallel. Work planned for the coming quarter includes measurements at elevated temperatures of the dynamic elastic constants of monocrystalline W, ZrC, and TiC and of polycrystalline ZrC and TiC.

X-ray techniques have been used to measure the thermal expansion and mean atomic-vibration amplitudes for TiC from 25° - 1700°C. The titanium and the carbon atoms seem to have the same mean vibration amplitudes. During the next quarter a new hot-zone assembly will be used to extend the thermal expansion data to higher temperatures, we hope to above 2000°C. Lattice expansion and atomic-vibration amplitudes will also be determined for ZrC.

Measurements of electrical resistivity and Hall effect have been made on single-crystal samples of TiC and on polycrystalline samples of ZrC and TiC from -269° to 40°C. The polycrystalline sample of TiC, hot-pressed from crushed single-crystal material, had a much lower resistivity than the single crystals, an interesting and unexplained result. Work during the next quarter will include measurements of the galvanomagnetic properties of ZrC single crystals and a solid solution of ZrC and TiC.

The equipment for tensile creep testing was used to test a steel specimen at about 800°C. In the immediate future creep tests will be made on tantalum samples to check operation of the equipment at higher temperatures. These will be followed by determinations of strength and ductility in creep as functions of temperature for various refractory carbides and borides. Specimens of commercial TiB_2 are on hand for testing.

Measurements of thermal conductivity have been completed on nine samples of GPF graphitized foam from the National Carbon Company. This foam, while having a high porosity, has a smaller maximum pore size than the GUF graphitized foam previously measured. This helps to suppress radiative heat transport at high temperatures. The results of these measurements fit nicely into the model developed to describe the GUF data. They are discussed in full in a report now being prepared.

The main effort on materials preparation during this quarter has been on the hot-pressing of samples for the gas-solid reaction work. Samples have

also been made for galvanomagnetic, x-ray, and elastic measurements. Additional work has been done to investigate the vacuum purification of carbides and borides. Special equipment has been ordered in which induction heating can be used for zone melting, zone sintering, drip melting, or levitation melting. During the coming months, work will be continued on sample preparation, with emphasis on larger specimens for measurements of thermal and mechanical properties, and on studies of vacuum purification of refractory carbides and borides.

II INTRODUCTION

This program is concerned with the principles governing high-temperature chemical and physical behavior, especially those behaviors contributing importantly to the successful performance of materials as rocket components operating at high temperatures.

The interaction of a rocket nozzle with its milieu can importantly affect its behavior. Corrosion and vaporization lead directly to loss of material and strength. Furthermore, if either acts selectively to produce cracklike structures or to accelerate crack growth by a stress-corrosion mechanism, its effect is greatly amplified in comparison to the amount of material removed. It is for these reasons that gas-solid reactions and vaporization are being studied in this program. In particular, a program of chemical screening tests has been inaugurated during this reporting period to give a general view of the relative resistance of refractory carbides and borides to important component gases of rocket exhausts and to mixtures of these. Since graphite and tungsten are important rocket-nozzle materials, they have also been subjected to the same tests to provide a basis of comparison.

As structural parts, rocket nozzles are subjected to substantial stresses during operation. Some of these stresses change relatively slowly with time, and their effects on the nozzle will be determined by the creep strength and ductility of the materials involved. There are also rapidly changing stresses resulting from sudden heating or cooling of the part. The resistance of the nozzle to such thermal shock will depend upon a combination of properties which it is enlightening to consider individually. The thermal stresses developed by a given temperature change increase with an increasing coefficient of expansion or elastic modulus, and they decrease with increasing thermal conductivity or specific heat. The ability to avoid fracture from these stresses depends upon the tensile strength and the ductility of the material. All these properties are being investigated for these reasons and some of them for others as well. Thus, a knowledge of the elastic modulus of his material is basic for any designer, and thermal conductivity and specific heat are necessary for calculations of heat transfer.

The major group of materials being studied here consists of the refractory carbides and borides of the transition metals. The technology of these materials is not well advanced, a neglect that has been largely a result of their brittleness at room temperature. Consequently a considerable effort is being devoted to the preparation of powders of these compounds with good purity and to their fabrication into test specimens without adulteration.

III TECHNICAL RESULTS AND PLANS

A. Gas-Solid Reaction Studies

1. Chemical Screening Tests — I. R. Ladd, J. R. McDowell, P. N. Walsh

An exploratory investigation has been undertaken of high-temperature chemical reactivity of solid materials with various corrosive species known or expected as combustion products from current or proposed rocket fuels. The primary aim is to obtain qualitative information on the relevant chemical stability of actual or prospective rocket-nozzle materials rather than detailed information of immediate applicability to rocket engineering. The nature and extent of the chemical reactions taking place, the mechanism of attack (i.e., grain boundary penetration, surface attack, etc.), the effects of sample purity, composition, and density, the dependence on gas composition, and the overall course of the reactions are all being followed. It is hoped that general patterns of behavior will be revealed that will be useful for predicting at least the relative chemical stabilities of the refractory materials in actual rocket application.

a. Experimental Results. The materials presently under investigation are the refractory carbides and borides, tungsten, and several types of graphite. The gases used so far are CO, CO_2, H_2, H_2O, HCl, and BF_3. It is not expected that more than one or two additional materials will enter the program, but other gases and gas mixtures will be included as seems appropriate, and reactions involving liquid Al_2O_3 will be studied.

A program of thermodynamic calculations has also been undertaken in support of the experimental work. The purpose of this program is to determine the kinds and amounts of product species to be expected, at equilibrium, from each of the reactions studied experimentally. While equilibrium conditions are not established in the experiments, these calculations are expected to aid in the interpretation of the observations since, at the high temperatures employed in this work, most thermodynamically possible reactions will actually proceed. Differences in reaction rates (unrelated to differences in free energy of reaction) may still be of the greatest importance, of course.

For convenience, a single temperature (3000°K) was assumed in the calculations, though the experiments have generally been run at various appreciably lower temperatures; the difference in temperature usually does not alter the qualitative conclusions drawn while necessary modifications (e.g. because different phases are stable at the different temperatures) are obvious.

Solid samples approximately 1/4 x 1/4 x 1/8 inch in size were heated in a partial atmosphere of the gas under study in an arc-image furnace. The container system, constructed of Pyrex and Tygon, could be evacuated to a pressure of less than 0.1 mm Hg. Each sample was supported at two opposite corners by a pair of holder arms made from the same material as the sample and mounted on a tantalum holder (see Fig. 1). The solid samples were situated at the near focus of the external elliptical mirror of the arc-image furnace. Nearly the entire front surface of the sample was in the beam. The earliest runs were made at the highest temperatures then attainable; it was later decided to keep the temperature in the more easily reproducible range 2100-2200°C (brightness temperature). Brightness temperatures were read with an optical pyrometer. A pair of synchronized rotating shutters was arranged so that the pyrometer, which was focused on the sample face exposed to the image furnace radiation, and arc were exposed to the sample alternately. The gas of interest was allowed to flow slowly through the experimental vessel; the pressure was maintained below atmospheric by throttled pumping. No attempt was made to simulate rocket-exhaust pressures or flow conditions.

In all cases, both the gases and solid samples were used as received without further purification. The gases were commercial materials at least 99% pure; the CO_2, H_2, and CO had purities better than 99.9%. The samples were hot-pressed bodies of 75% or higher theoretical density and 95% or higher purity.

The hot-pressed samples were ground with a diamond wheel to have flat, parallel faces. Before and after each experiment the sample was weighed and measured.

The experimental conditions and derived corrosion data are shown in Table I. For each solid-gas combination studied, the reaction time, temperature, initial bulk density of the solid, and initial and final pressures in the

reaction vessel are shown (for more precise definition of these parameters see notes in Table A-I). In the sixth column are listed the observed rates of weight change (as a function of surface area, because not all samples were the same size). The ratio of this figure to the initial weight of the sample is listed in the seventh column because it is felt that expressing the data in this form gives a truer picture of the relative rates of degradation of materials of such widely differing densities as those studied here. For those samples which did not suffer a gross change in shape, a "corrosion rate" (in mils/sec.) was calculated from the observed weight changes and bulk densities, assuming uniform attack on all surfaces of the sample; this is listed in the eighth column. In the last column, a brief description of the appearance of the sample surface after the reaction is given; where gas mixtures were used, the composition of the mixture is also given in this column.

b. Conclusions. The figures in the seventh column of Table A-I are regrouped by material and by reactant gas in Table A-II to facilitate evaluation of the results. Comparisons should be made with due regard for the differences in temperature between experiments. Small differences in absolute values should not be considered significant because appreciable uncontrolled variations of sample porosity and purity, gas purity and flow rate, temperature, etc. surely occurred. It is only when a definite trend is evident in the behavior of a particular material or group of materials that the results are meaningful. With these restrictions understood, the data in Table A-II would appear to support the following conclusions:

1. Neither CO nor H_2 reacts to any large extent with the materials used here. The latter reacted appreciably only with graphite. Attack by CO was somewhat greater, considering the temperatures employed, on the borides than on the carbides. These observations are in agreement with the qualitative results of the thermodynamic calculations, which indicate that hydrogen should react with graphite more than with the stabilized carbon in the carbides (see also Section A.2. which indicates that reaction mechanism in the two cases may be quite different) and hardly at all with the metal borides, while CO should attack only the borides, forming gaseous BO. The relatively large weight losses with TSX and SPK graphite in CO cannot be explained

readily, but may be due to residual oxygen in the system during these particular experiments.

2. Carbon dioxide and water are very strong oxidizers at high temperatures. (They are expected, from thermodynamic considerations, to attack all the materials studied here.) Reaction indeed was great; with the tantalum and niobium compounds complete collapse of the samples was observed in some cases, presumably due to formation of the relatively low-melting metal oxides. The borides of these metals stood up better than the carbides, though melting, at least of the surface, was observed in each case. The greater apparent stability of the borides could arise from formation of relatively stable high-melting borates (some weight gains were observed), but no direct evidence for the formation of such compounds has been obtained. The titanium compounds lost weight and showed signs of partial melting, while adherent coatings were formed on the zirconium compounds. This behavior is entirely consistent with the melting points and volatilities of the oxides of these metals. Under the conditions of these experiments, tungsten clearly outperformed all the other materials in oxidizing atmospheres.

3. Interpretation of the results obtained with HCl and BF_3 is complicated by the occurrence of side reactions involving the tantalum sample holders. Apparently these sample holders were attacked with the formation of volatile tantalum halides which subsequently decomposed on the sample surfaces. Spectrographic analyses of scrapings from the surface of the ZrB_2 and TiB_2 samples used in the HCl reactions revealed substantial amounts of tantalum. In addition, it was noted that tantalum was a major component of the solid deposited on the reactor wall when TiB_2 was allowed to react with HCl or BF_3.

If it can be assumed that this effect, though serious, does not completely invalidate the results, a reasonable picture of the chemistry involved can be derived from these experiments, though the weight gains noted for CbC in HCl and for SPK graphite in BF_3 are certainly anomalous. The relevant (diatomic and triatomic) gaseous zirconium halides are known to be more stable than their

titanium analogs, and, though the data are far from complete, are almost certainly considerably more stable than the halides of the heavier metals. The effect of this is apparent in the high weight losses observed for ZrC and ZrB_2 in HCl and for ZrB_2 in BF_3; ZrC in BF_3 did not show this, but the high temperature used may have resulted in the deposition of an unusual amount of tantalum. The borides are expected to be more readily attacked than the corresponding carbides, due to formation of the very stable molecule BF, and the experiments appear to verify this in a general way, except for the tantalum compounds. Graphite should be much more stable than the carbides in BF_3 because the attack by this gas is expected to be directed chiefly toward the metal atoms in the carbide (gaseous carbon fluorides are much less stable than gaseous ZrF and ZrF_2, for example, at high temperatures) and the experiments appear to confirm this also. Tungsten is seen to be about on a par with the best other materials in each atmosphere.

4. In a general way, there appears to be a correlation between the thermodynamic calculations and the extent of reaction observed in these experiments; i.e., the extent of reaction is greater the higher the calculated equilibrium partial pressure of products. While this correlation is far from perfect, if it can be substantiated it would make a useful qualitative working guide for choosing materials. Studies to test the extent to which such a correlation is useful are planned.

c. Future Work. Plans for further studies of these and similar gas-solid reactions during the next quarter are listed below.

1. The effect of varying partial pressures of the active gases both in inert diluents and in diluents of opposite chemical character (e.g., CO_2 in CO and H_2O in H_2) will be investigated.

2. Work will be initiated with HF and possibly with gaseous $AlCl_3$ and liquid Al_2O_3.

3. Some studies at higher temperatures will be started, using a current-concentrator induction furnace presently under construction.

4. The effect of mixing gases will be investigated. Of primary interest here are mixtures where one gas (HF) might attack the product (e.g., ZrO_2) from another gas (CO_2).

5. Reaction mechanisms will be examined more closely by the following means:

a) Metallographic examination of the samples after reaction to determine mode of penetration.

b) Weight loss and related measurements (including metallographic) on single crystals or at least samples with only a small number of grain boundaries as well as on purified and densified materials.

c) Determination of reaction products by x-ray (for solids) and gas analysis, and determination of the rates of formation of these products.

FIGURE A - 1

HOLDER USED FOR REACTIONS PERFORMED IN ARC - IMAGE FURNACE

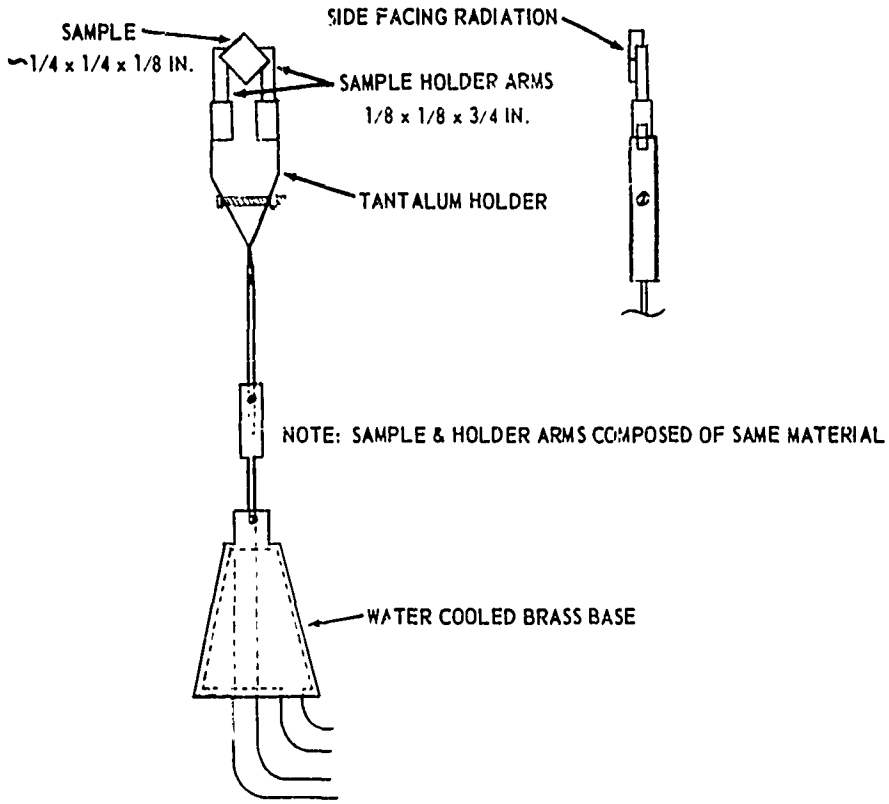

TABLE A-I

Reaction	Time Min.	Temp.[1]* °C	Press[2] mm	Bulk[3] Density g/cm³	Wt. Change[4] Rate x 10^{-4} gc/cm²/min.	Wt. Change[5] Rate Ratio x 10^{-4} gc/g/cm²/min.	Corrosion[6] Rate x 10^{-4} mils/sec.	Comments[7]
TiB_2 + CO	2.75	2050	608-618	4.1	+ 0.65	+ 1.1	---	Blue-grey surface
TiB_2 + CO_2	3.5	2030	632-690	4.1	- 390	- 730	620	Melted surface
TiB_2 + CO/H_2O[7]	3.0	2290	26-28	4.1	- 120	- 320	240	CO/H_2O = ~1 Melted surface
TiB_2 + H_2	5.0	2170	564-598	4.0	- 0.27	- 0.60	0.44	Silvery surface
TiB_2 + HCl	4.5	2100	700-600	4.3	- 24	- 45	37	Thin gold coating
TiB_2 + BF_3	3.7	2200	492-582	4.1	- 96	- 183	160	Grey surface
ZrB_2 + CO	5.0	2400	570-592	5.5	- 8.3	- 14	8.8	Volume increased 11%. Blue-grey surface
ZrB_2 + CO_2	3.5	2600	484-540	5.8	+ 34	+ 63	--	White coating
ZrB_2 + CO/CO_2	6.0	2000	502-610	5.2	+ 5.9	+ 10	--	CO/CO_2 = 9.5 White coating
ZrB_2 + CO/H_2O	5.0	2700	-	5.6	+ 4.0	+ 7.1	---	Water vapor ~15 mm Thick coating
ZrB_2 + H_2	5.0	2430	618-650	5.4	- 5.1	- 10	6.1	Silvery surface
ZrB_2 + HCl	4.5	2000	466-364	5.7	- 180	- 320	200	Thin gold coating
ZrB_2 + BF_3	3.8	2350	314-346	5.5	- 230	- 450	260	Grey surface
CbB_2 + CO	4.5	2370	626-646	4.8	- 1.4	- 2.7	1.8	
CbB_2 + CO_2	3.0	2200	636-658	5.6	+ 40	+ 46	--	Sample melted

* See notes at end of Table A-1

TABLE A-I (Continued)

Reaction	Time Min.	Temp.[1] °C	Press[2] mm	Bulk[3] Density g/cm³	Wt. Change[4] Rate x 10^{-4} gc/cm²/min.	Wt. Change[5] Rate Ratio x 10^{-4} gc/g/cm²/min.	Corrosion[6] Rate x 10^{-4} mils/sec.	Comments[7]
CbB_2 + CO/H_2O	4.5	2260	224-232	5.4	+ 3.3	+ 4.4	--	CO/H_2O ~ 10 Melted surface
CbB_2 + H_2/H_2O[8]	4.0	2200	219-306	5.4	- 41	- 52	49	H_2/H_2O ~ 15 Melted surface
CbB_2 + H_2	4.5	2220	625-630	5.6	+ 1.2	+ 1.5	--	
CbB_2 + HCl	4.5	2280	590-630	5.1	- 27	- 58	35	Dull tan porous surface
CbB_2 + BF_3	4.5	2260	655-670	5.4	- 46	- 63	56	Yellow-tan porous surface
TaB_2 + CO	4.5	2300	630-640	10.5	- 5.9	- 5.0	3.7	Silvery surface
TaB_2 + CO_2	3.0	2240	636-658	10.4	~30% volume loss		--	Fused to holder
TaB_2 + CO/H_2O	4.5	2240	218-232	10.2	- 3.8	- 2.4	2.4	CO/H_2O ≈ 14 Melted surface
TaB_2 + H_2H_2O	4.5	2230	210-266	10.0	+ 10	+ 6.9	--	H_2/H_2O ~ 14 Melted surface
TaB_2 + H_2	4.5	2250	626-640	9.8	- 2.1	- 1.4	1.9	Silvery surface
TaB_2 + HCl	3.6	2230	605-640	10.4	- 95	- 60	60	Yellow-brown surface film
TaB_2 + BF_3	4.5	2240	640-655	10.0	- 50	- 35	33	Dull tan surface coating
TiC + CO	4.5	2700	638-670	4.6	- 2.8	- 4.5	3.9	
TiC + CO_2	1.0	2[illegible]	156-158	4.6	- 380	- 830	540	Melted surface
TiC + CO/H_2O	5.0	2240	32-42	4.4	- 220	- 410	320	CO/H_2O ~ 3 Melted surface

TABLE A-I (Continued)

Reaction	Time Min.	Temp.[1] °C	Press[2] mm	Bulk[3] Density g/cm³	Wt. Change[4] Rate x 10^{-4} gc/cm²/min.	Wt. Change[5] Rate Ratio x 10^{-4} gc/g/cm²/min.	Corrosion[6] Rate x 10^{-4} mils/sec.	Comments[7]
TiC + H_2/H_2O	3.0	2230	218-224	4.8	- 110	- 180	155	H_2/H_2O ~ 14 Melted surface
TiC + H_2	5.0	2470	552-530	4.6	- 2.6	- 4.9	3.7	
TiC + HCl	4.5	2450	444-286	4.6	- 19	- 31	27	Gold surface film
TiC + BF_3	4.5	2350	550-530	4.5	- 39	- 68	57	Yellow-brown surface
ZrC + CO	8.3	2700	545-637	6.4	- 1.9	- 3.4	2.0	
ZrC + CO_2	4.5	2500	596-624	6.6	+ 120	+ 190	--	Thick white coating
ZrC + CO/CO_2	8.5	2000	502-582	6.4	+ 18	+ 36	--	CO/CO_2 = 9.4 White coating
ZrC + CO/H_2O	5.0	2460	218-232	6.4	+ 30	+ 38	--	CO/H_2O ~ 14 Thin greyish coating
ZrC + H_2	5.0	2300	478-408	6.2	- 2.3	- 3.6	2.5	
ZrC + HCl	5.0	2100	484-376	6.4	- 37	- 70	38	
ZrC + BF_3	3.5	2500	326-420	5.5	- 40	- 67	48	
CbC + CO	4.5	2700	562-558	6.3	- 0.16	- 0.24	0.16	
CbC + CO_2	2.5	2700	222-228	6.1	unweighable	~1/2 reacted	--	
CbC + CO/H_2O	2.7	2250	84 steady	5.9	unweighable	~1/3 reacted	--	CO/H_2O ~ 5 Sample melted
CbC + H_2	5.0	2500	288-314	5.9	- 2.9	- 4.7	3.2	Silvery surface

TABLE A-I (Continued)

Reaction	Time Min.	Temp.[2] °C	Press[2] mm	Bulk[3] Density g/cm³	Wt. Change[4] Rate x 10^{-4} gc/cm²/min.	Wt. Change[5] Rate Ratio x 10^{-4} gc/g/cm²/min.	Corrosion[6] Rate x 10^{-4} mils/sec.	Comments[7]
CbC + HCl	3.8	2500	700-560	6.2	+ 1.2	+ 1.5	--	
CbC + BF_3	4.5	2050	392-520	6.1	- 5.8	- 7.7	6.2	
TaC + CO	5.0	2300	594-616	12.3	- 1.5	- 0.89	0.81	Yellow-brown surface
TaC + CO_2	3.5	2250	610-662	12.1	unweighable	~1/3 reacted	--	Sample melted
TaC + CO/H_2O	2.0	2250	32 steady	12.1	- 340	- 240	180	CO/H_2O ~ 2 Thin glassy coating
TaC + H_2/H_2O	3.0	2230	218-222	11.5	- 13	- 15	8.4	H_2/H_2O ~ 14
TaC + H_2	5.0	2100	618-596	12.0	+ 0.76	+ 0.67	--	Yellow-grey surface
TaC + HCl	4.5	2200	790-736	12.0	- 55	- 41	30	Dull gold surface
TaC + BF_3	4.5	2190	600-628	12.8	- 57	- 39	29	Grey surface
AGOT + CO	3.0	2300	594-608	1.6	- 1.0	- 5.1	4.3	
AGOT + CO_2	2.5	2320	644-666	1.7	- 220	-1100	860	Black crumbly surface
AGOT + CO/H_2O	3.0	2270	26-25	1.7	- 39	- 190	150	CO/H_2O ~ 1 Porous surface
AGOT + H_2	4.5	2250	672-656	1.7	- 3.2	- 15	12	
AGOT + HCl	4.5	2150	528-466	1.8	- 0.89	- 4.3	3.2	Gold film on surface
AGOT + BF_3	4.5	2370	650-750	1.7	- 1.2	- 6.1	4.6	Black porous surface

TABLE A-I (Continued)

Reaction	Time Min.	Temp.[1] °C	Press[2] mm	Bulk[3] Density g/cm³	Wt. Change[4] Rate x 10^{-4} gc/cm²/min.	Wt. Change[5] Rate Ratio x 10^{-4} gc/g/cm²/min.	Corrosion[6] Rate x 10^{-4} mils/sec.	Comments[7]
AGKSP + CO	4.2	2350	620-612	1.7	none	none	none	
AGKSP + CO_2	2.9	2200	602-614	1.6	- 200	-1000	930	Black crumbly surface
AGKSP + CO/H_2O	3.0	2285	26 steady	1.7	- 65	- 320	250	CO/H_2O ~ 1 Porous surface
AGKSP + H_2	4.5	2200	612-604	1.6	- 5.8	- 28	24	
AGKSP + HCl	4.5	2250	654-564	1.7	- 2.0	- 10	7.8	Yellow-brown surface film
AGKSP + BF_3	4.5	2310	572-622	1.7	- 1.6	- 8.1	6.2	
ATJ + CO	4.5	2380	662-676	1.8	- 0.41	- 1.9	1.6	
ATJ + CO_2	2.1	2300	654-676	1.8	- 260	-1200	940	Black crumbly surface
ATJ + CO/H_2O	3.0	2280	28 steady	1.8	- 57	- 270	210	CO/H_2O ~ 1 Porous surface
ATJ + H_2/H_2O a.	3.0	2240	226-230	1.8	- 52	- 260	190	H_2/H_2O ~ 12 Porous surface
ATJ + H_2/H_2O b.	3.0	2250	24 steady	1.8	- 68	- 320	240	H_2/H_2O ~ 1 Porous surface
ATJ + H_2	4.5	2330	606-594	1.8	- 5.6	- 25	21	
ATJ + HCl	3.5	2200	574-614	1.9	- 5.2	- 25	18	
ATJ + BF_3	4.5	2330	578-624	1.8	- 0.29	- 1.3	1.0	

TABLE A-I (Continued)

Reaction	Time Min.	Temp.[1] °C	Press[2] mm	Bulk[3] Density g/cm^3	Wt. Change[4] Rate x 10^{-4} gc/cm^2/min.	Wt. Change[5] Rate Ratio x 10^{-4} gc/g/cm^2/min.	Corrosion[6] Rate x 10^{-4} mils/sec.	Comments[7]
TSX + CO	4.5	2280	608-522	1.9	- 3.0	- 14	10	
TSX + CO_2	3.0	2430	596-566	1.8	- 210	- 970	730	Black crumbly surface
TSX + H_2	4.5	2290	616-500	1.9	- 8.1	- 39	29	Black porous surface
TSX + HCl	4.5	2230	660-450	1.9	- 5.6	- 26	20	Porous surface
TSX + BF_3	4.5	2240	660-556	1.9	- 2.1	- 10	7.4	Yellow-tan surface film
SPK + CO	4.2	2550	616-642	1.9	- 4.7	- 22	16	
SPK + CO_2	1.7	2270	570-556	1.8	- 200	- 910	700	Black porous surface
SPK + CO/H_2O	3.0	2290	24 steady	1.9	- 45	- 200	150	$CO/H_2O \sim 1$ Porous coating
SPK + H_2 a.	4.5	2550	640-629	2.0	- 31	- 140	100	Black porous surface
SPK + H_2 b.	4.5	2350	572-560	1.9	- 12	- 56	43	Black porous surface
SPK + HCl	2.3	2200	482-456	2.0	- 2.2	- 11	7.2	Yellow-brown surface coating
SPK + BF_3	4.5	2440	584-616	1.9	+ 1.6	+ 7.5	--	
ZTA + CO	4.5	2420	654-664	2.0	- 0.72	- 2.9	2.3	
ZTA + CO_2	2.0	2360	596-628	2.2	- 250	- 990	730	Black crumbly surface
ZTA + CO/H_2O	3.0	2270	25-26	2.0	- 56	- 220	180	$CO/H_2O \sim 1$ Porous surface

TABLE A-I (Continued)

Reaction	Time Min.	Temp.[1] °C	Press[2] mm	Bulk[3] Density g/cm^3	Wt. Change[4] Rate x 10^{-4} gc/cm^2/min.	Wt. Change[5] Rate Ratio x 10^{-4} gc/g/cm^2/min.	Corrosion[6] Rate x 10^{-4} mils/sec.	Comments[7]
ZTA + H_2/H_2O a.	3.0	2230	220-226	2.0	- 28	- 110	93	H_2/H_2O ~ 10 Porous surface
ZTA + H_2/H_2O b.	3.0	2290	27-26	2.1	- 47	- 190	150	H_2/H_2O ~ 1 Porous surface
ZTA + H_2	4.5	2370	556-564	2.0	- 4.4	- 18	14	Black porous surface
ZTA + HCl	4.5	2200	564-504	2.1	- 3.1	- 13	9.7	Yellow surface film
ZTA + BF_3	4.5	2320	600-634	2.0	- 3.2	- 13	10	Black porous surface
W + CO	4.5	2220	613-632	20.9	- 2.9	- 1.2	0.90	Gold surface film
W + CO_2	4.5	2220	650-630	20.6	- 230	- 110	74	Gold surface film
W + CO/H_2O	4.5	2240	224-230	20.4	- 47	- 24	15	CO/H_2O ~ 12 Gold surface
W + H_2/H_2O	4.5	2220	217-219	20.7	- 1.2	- 0.52	0.38	H_2/H_2O ~ 12
W + F_2	4.5	2240	622-628	20.3	- 1.1	- 0.48	0.37	
W + HCl	4.5	2230	600-550	20.8	- 13	- 5.7	4.2	
W + BF_3	4.5	2240	628-666	20.5	- 48	- 20	15	
W + HF	2.2	2200	600-720	20.5	- 6.2	- 2.7	2.0	

NOTES:

1. These are brightness temperatures. During a run variations of 50°C from the recorded temperature were frequently observed.
2. Initial and final pressure readings are listed in that sequence for all gases except HCl. In the HCl reactions irregular fluctuations in pressure were caused partially by unsteady output from the cylinder. In all other cases pressure changes were caused mainly by thermal or chemical effects inherent in the experiment.
3. The bulk density of each solid piece was calculated from weight and dimension measurements.
4. Weight change rate = grams change (gain or loss)/cm^2/min.
5. Weight change rate ratio = grams change (gain or loss)/grams total (initially)/cm^2/min.
6. Corrosion rate = $$\frac{\text{weight loss(g) x 394 mil/cm}}{\text{Bulk density}\left(\frac{\text{g}}{\text{cm}^3}\right) \text{ x area } (\text{cm}^2) \text{ x time (sec.)}}$$
7. Comments pertain to appearance of solid samples after reaction.
8. All CO/H_2O and H_2/H_2O, experiments were performed by bubbling CO or H_2 through distilled water at room temperature, then passing the vapor mixture over the hot sample.

TABLE A-II

COMPOUND	CO		CO_2		CO/H_2O		H_2		HCl		BF_3	
	Temp. (°C)	Ratio[1] ($x10^4$)	Temp. (°C)	Ratio ($x10^4$)	Temp. (°C)	Ratio ($x10^4$)	Temp. (°C)	Ratio ($x10^4$)	Temp. (°C)	Ratio ($x10^4$)	Temp. (°C)	Ratio ($x10^4$)
TiB_2	2050	+ 1.1	2030	- 730	2290	- 320	2170	- 0.60	2100	- 45	2200	- 183
ZrB_2	2400	- 14	2600	+ 63	2700	+ 7.1	2430	- 10	2000	- 320	2350	- 450
CbB_2	2370	- 2.7	2200	+ 46	2260	+ 4.4	2220	+ 1.5	2280	- 58	2260	- 63
TaB_2	2300	- 5.0	2240	- 1/3[2]	2240	- 2.4	2250	- 1.4	2230	- 60	2240	- 35
TiC	2700	- 4.5	2320	- 830	2240	- 410	2470	- 4.9	2450	- 31	2350	- 68
ZrC	2700	- 3.4	2500	+ 190	2460	+ 38	2300	- 3.6	2100	- 70	2500	- 67
CbC	2700	- 0.24	2700	- 1/2[2]	2250	- 1/3[2]	2500	- 4.7	2500	+ 1.5	2050	- 7.7
TaC	2300	- 0.89	2250	- 1/3[2]	2250	- 240	2100	+ 0.67	2200	- 41	2190	- 39
ATJ Graphite	2380	- 1.9	2300	-1200	2280	- 270	2330	- 25	2200	- 25	2330	- 1.3
TSX Graphite	2280	- 14	2430	- 970	--	--	2290	- 39	2230	- 26	2240	- 10
SPK Graphite	2550	- 22	2270	- 910	2290	- 200	2550 2350	- 110 - 56	2200	- 11	2440	+ 7.5
ZTA Graphite	2420	- 2.9	2360	- 990	2270	- 220	2370	- 18	2200	- 13	2320	- 13
W	2220	- 1.2	2220	- 110	2240	- 24	2240	- 0.48	2230	- 5.7	2240	- 20

NOTES: 1. Ratio = Weight change rate ratio ($gc/g/cm^2/min$)
2. Estimated volume decrease; the reacted sample was unweighable.

2. Quantitative Kinetic Studies

J. R. McDowell

Further experiments on the hydrogen-graphite reaction have been conducted to determine the effects of variation of gas pressure at constant graphite temperature and to study the rate of production of propane as function of graphite temperature between 1800°C and 2500°C. The same type of liquid-nitrogen-cooled reactor has been used in preliminary experiments on the reaction of hydrogen with TiC. Studies have been initiated to elucidate the mechanism of production of acetylene in the hydrogen-graphite reaction by using a mixture of hydrogen and deuterium and determining the abundances of the isotopic species C_2H_2, C_2HD, and C_2D_2.

a. Reaction of Hydrogen and Graphite. The zero-time rates of production of methane and of acetylene at 2150°C are at least roughly first-order with respect to hydrogen pressure in the range 3.5 - 12.2 mm, as shown in Figure A-2. The time rates R_o were obtained by graphical extrapolation of data for rate versus time at constant pressure. As explained in former reports, R_o values are measured in order to remove the effect of pyrolysis of methane. At 2150°C, the rate constant for methane, determined from the limited amount of data, was 6.2×10^{-10} moles/cm^2 of graphite surface/mm. H_2 pressure/sec; for acetylene it is 2.3×10^{-10} moles/cm^2/mm/sec.

The rate of production of propane has been studied from 1800 to 2500°C at a hydrogen pressure of 4.5 ± 0.2 mm. The temperature dependence of R_o is shown in Figure A-3, and an Arrhenius plot of the data in Figure A-4. The sharp break in the latter plot at about 2050°C is believed to indicate that a new mechanism becomes dominant above this temperature. If the rates for the low temperature process (whatever the mechanism) are extrapolated linearly on the Arrhenius plot to higher temperatures and subtracted from the observed overall rates, the activation energy for the high temperature process is found to be 187 kcal/mole. The agreement between this value and the 185 kcal/mole reported for the heat of sublimation of graphite to C_3 at 2500°K [1] indicates

(1) J. Drowart et al., J. Chem. Phys. 31, 1131 (1959).

that vaporization of C_3 may be the rate-controlling step in the formation of propane at high temperatures. (The amount of propane collected is about 20-25% of the estimated amount of C_3 vaporized.) The agreement in these heats, however, is undoubtedly better than is to be expected from the precision of our data; for example, in the case of two mechanisms operating simultaneously, as postulated here, a region of curvature should be observable between the two straight line segments of a plot like Figure A-4.

Reactions of mixtures of H_2 and D_2 with graphite can give information on mechanisms of formation of acetylene. If an acetylene molecule is formed by a process involving a single hydrogen molecule, only C_2H_2 and C_2D_2, but no C_2HD should be formed. If, however, the process involves two different hydrogen molecules, or if it involves hydrogen atoms, C_2HD should also be formed; with equal amounts of H_2 and D_2, in the absence of isotope effects, the ratios C_2H_2: C_2HD: C_2D_2 should be 1:2:1. On the basis of a single mass spectroscopic analysis for such a run, the ratio C_2H_2: C_2HD was 1:2. A more complete study should be made, especially to check on whether the hot carbon surface causes preliminary isotopic equilibration of the molecular hydrogen.

b. Reaction of Hydrogen and TiC. A preliminary experiment has been run to determine the products of reaction of TiC with hydrogen. A TiC rod was heated by resistance to 2100°C in a liquid-nitrogen-cooled reaction cell, and the gaseous products were analysed by gas chromatography. The main product was methane, and no acetylene was produced. Thus, there seems to be an important difference between the reaction of hydrogen with graphite and with TiC (and possibly other carbides as well).

c. Future Plans. Two types of investigations are proposed for future work. The first is a characterization of the gaseous products of reactions between refractory compounds and various gases. This will follow up the reaction studies made with the arc-image furnace. The second will consist of kinetic studies of the reactions of a variety of rocket exhaust components with carbides and borides.

FIGURE A - 2.
ZERO TIME RATE OF PRODUCTION OF METHANE AND ACETYLENE VERSUS HYDROGEN PRESSURE AT GRAPHITE TEMPERATURE OF 2150°C.

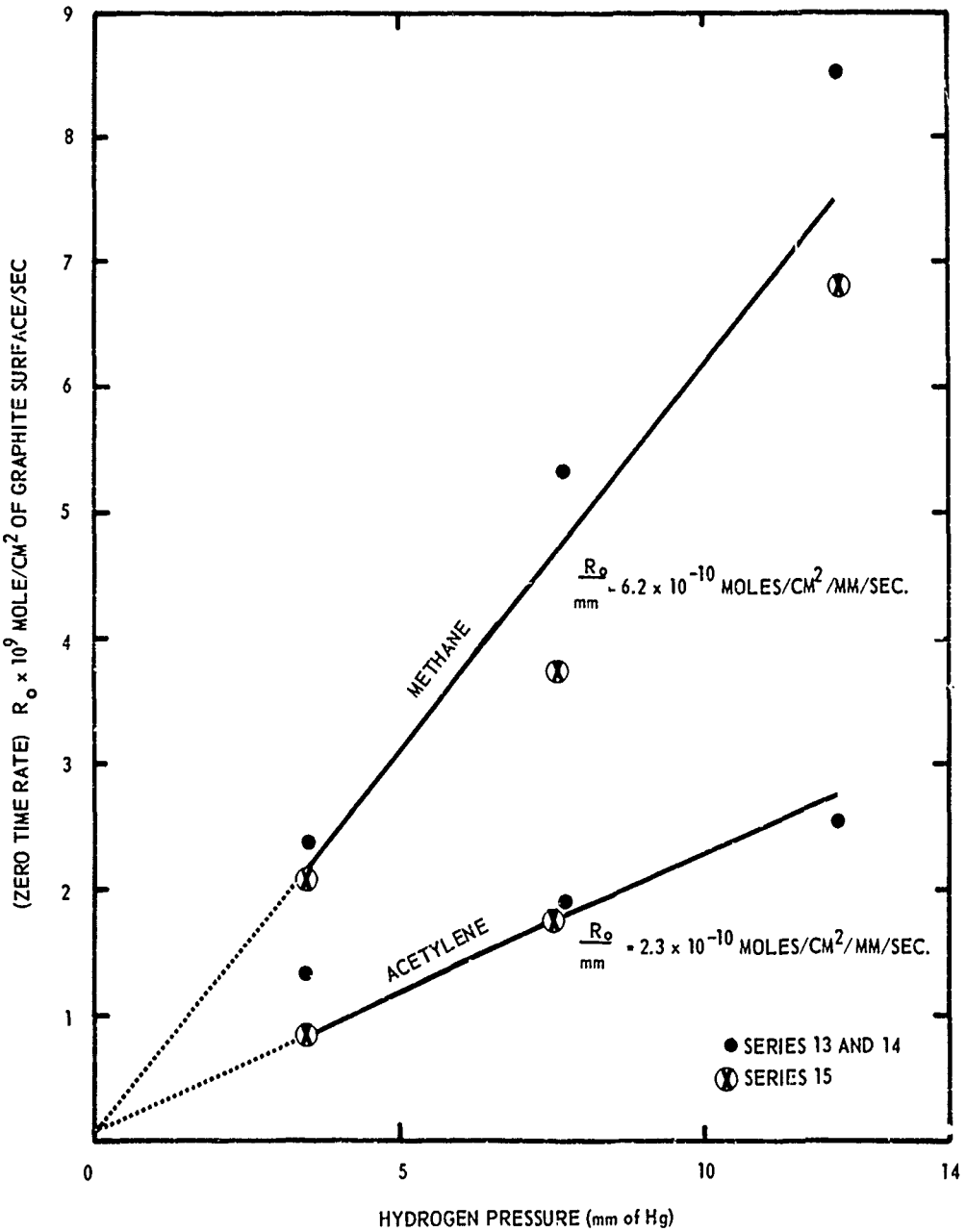

FIGURE A-3

ZERO TIME RATE OF PRODUCTION OF PROPANE VERSUS TEMPERATURE AT A HYDROGEN GAS PRESSURE OF 4.5±0.2 MM. H_g.

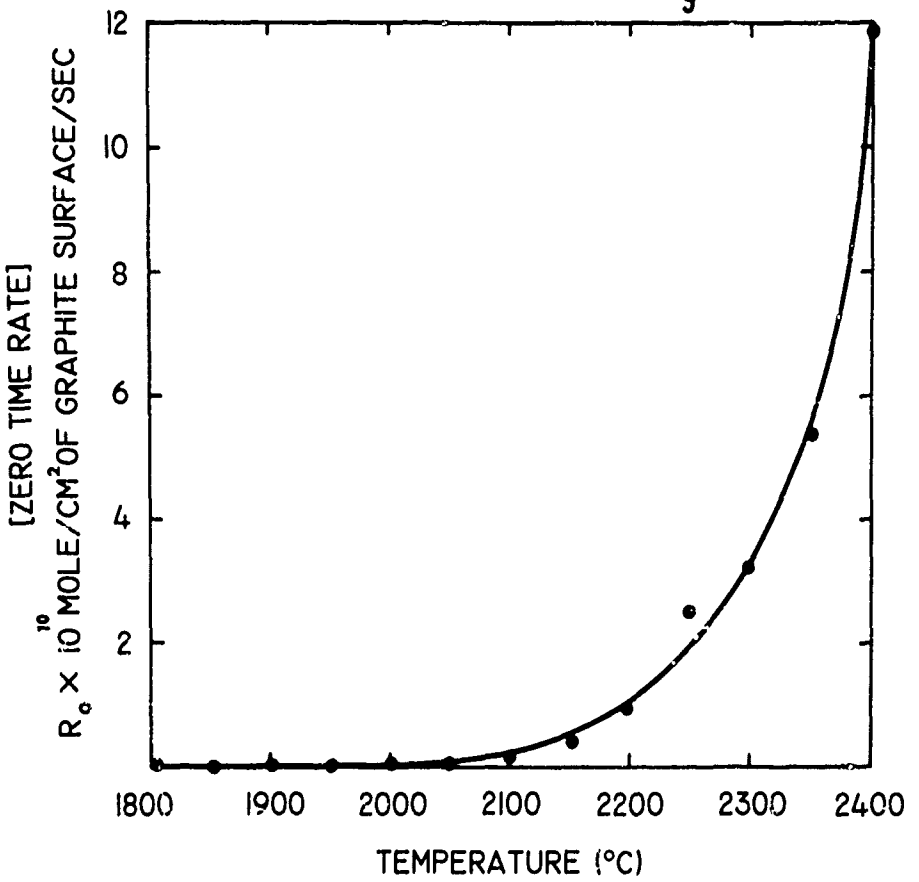

FIGURE A-4. LOG R_0 VERSUS $\frac{1}{T}$ FOR PROPANE

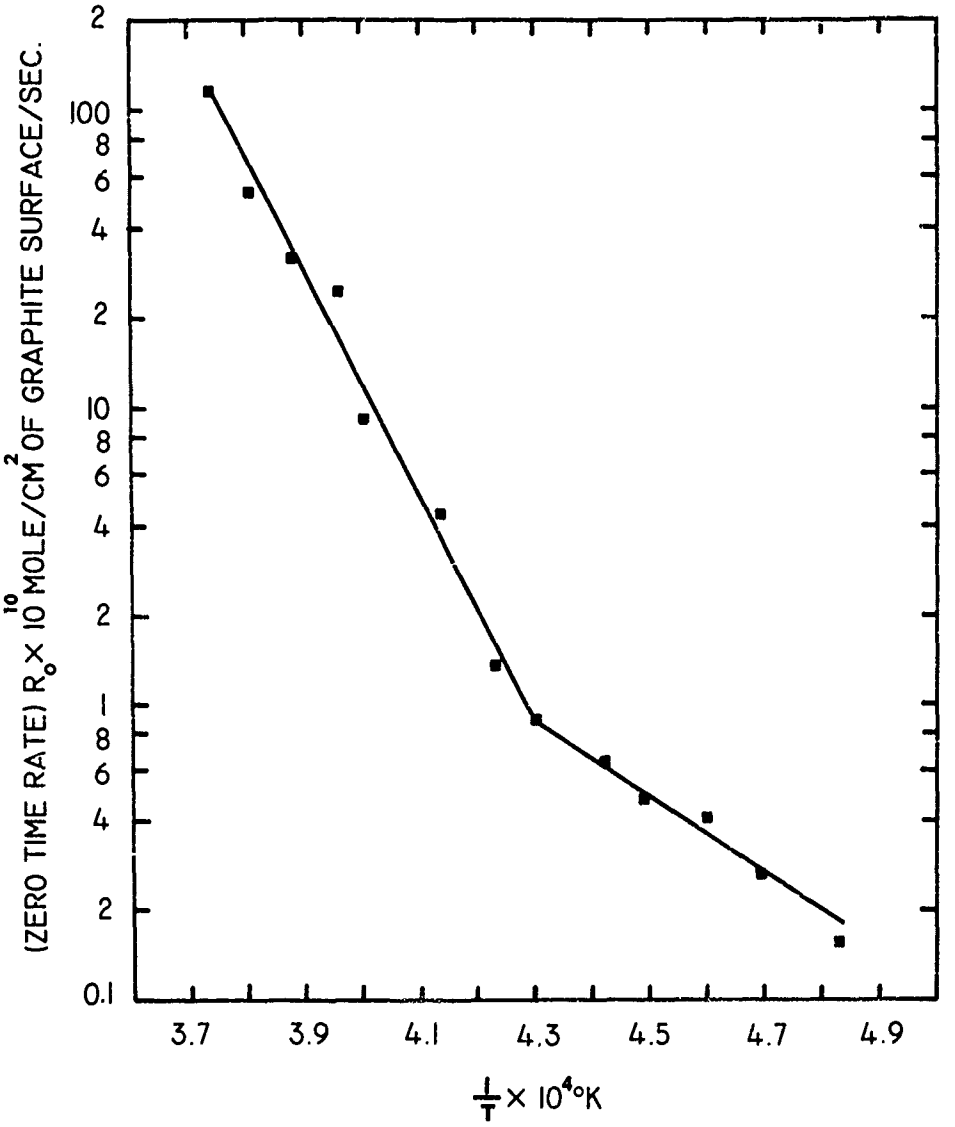

B. Thermodynamics and Kinetics of Vaporization

1. Mass Spectrometer Studies

H. W. Goldstein, O. C. Trulson

A 12-inch-radius, 60°-sector mass spectrometer built by Nuclide Analysis Associates has been installed during this period. This instrument will be used for high-temperature studies of vaporization phenomena and gas-solid reactions. Preliminary Knudsen effusion experiments have been performed in order to gain familiarity with the instrument and to assure its satisfactory operation. The Knudsen-cell source provided with the instrument has been modified so that it can be operated continuously above 2400°C.

a. Vaporization of ZrB_2. Preliminary high-temperature vapor-pressure data have been obtained for the thermal decomposition of powdered ZrB_2 samples according to the reaction

$$ZrB_2(s) \longrightarrow Zr(g) + 2B(g) \qquad (1)$$

where (s) and (g) refer to condensed and gas phases respectively. The first measurements were made with the sample loaded in a graphite effusion cell. At 2400°K the measured boron pressure was 1×10^{-5} atmospheres, while the level of the zirconium signal was below the sensitivity limit of the instrument with this Knudsen cell ($\sim 10^{-9}$ atmos.). This indicated a reaction with the crucible, since ZrB_2 is expected to vaporize nearly congruently. Such a reaction has been proposed by Leitnaker[2] for this system, viz.

$$ZrB_2(s) + C(s) \longrightarrow ZrC(s) + 2B(g), \qquad (2)$$

despite the positive free-energy change predicted for the all-solid reaction

$$ZrB_2(s) + C(s) \longrightarrow ZrC(s) + 2B(s). \qquad (3)$$

---

(2) J. M Leitnaker, "Thermodynamic Properties of Refractory Borides," LA-2402, TID-4500, 15th ed., Los Alamos Scientific Laboratory, April 1960.

A heat formation (ΔH^f_{298}) for $ZrB_2(s)$ of approximately -60 kcal/mole is calculated from a combination of the measured boron pressure and the heats of formation of ZrC(s)[3] and B(g)[4].

A second set of measurements was made with ZrB_2 inside a tantalum crucible lined with tungsten sheet to prevent physical contact between the tantalum and the ZrB_2 sample. Seven vapor-pressure measurements were made in the temperature range 2273 to 2556°K, and the zirconium and boron pressures were found to be of the same magnitude. An average heat of vaporization (ΔH^v_{298}) of approximately 460 kcal/mole was obtained which leads to a heat of formation (ΔH^f_{298}) of approximately -53 kcal/mole for ZrB_2. (Since these results are preliminary no detailed error analyses have been made; the expected error is of the order ± 10 kcal/mole.) Near 2400°K there was a sudden decrease in the intensities of the zirconium and boron signals, and inspection of the crucible and contents after the runs revealed considerable reaction at the ZrB_2 - tungsten interface. These preliminary data support the results by Leitnaker[2] for the vaporization of ZrB_2, although the heat of formation does not agree with the result of Huber, Head, and Holley,[5] ΔH_f = -77 kcal/mole, which Leitnaker assumed was correct.

More experimental data will be taken with graphite and tungsten crucibles to obtain a more reliable heat of vaporization. Since several investigators have obtained consistent results for the heat of vaporization of boron, a value near 132 kcal/mole will be assumed correct. There is some question as to the value for zirconium, and this must be known to obtain the heat of formation from the heat of vaporization of ZrB_2. Experimental measurements are being considered for determination of the heat of vaporization of zirconium from its vapor pressure.

---

(3) O. Kubaschewski and E. Evans, Metallurgical Thermochemistry, John Wiley and Sons, Inc., New York, 1956.

(4) JANAF Interim Thermochemical Tables, the Dow Chemical Company, Midland, Michigan, Dec. 31, 1960.

(5) E. J. Huber, E. S. Head, and C. Holley, Unpublished work cited in (2).

b. Future Work. The results of this early study of the high-temperature vaporization of ZrB_2 have demonstrated the satisfactory operation of the mass spectrometer. More work is planned on this compound. Simultaneously, experimental equipment will be assembled to study gas-solid reactions at high temperatures. Plans for equilibrium gas-solid reaction experiments involve admitting permanent gases to a crucible containing refractory carbides or borides and measuring the equilibrium concentration of the molecular species formed. Kinetic studies are also being considered in which a molecular beam would impinge upon a heated refractory target. The molecular species formed would be monitored with the mass spectrometer.

2. Matrix-Isolation Studies — P. N. Walsh, W. Weltner, Jr.

Molecular species evaporating from hot solids (for example B_2O_3 or C_3) can be identified by mass spectroscopy, but knowledge of their vibrational and electronic properties and their structures is more difficult to obtain. Calculation of the thermodynamic properties of these molecules (such as are found in the JANAF Tables) requires this additional information, which is clearly also desirable for understanding the fundamental behavior of these species in chemical reactions or when subject to absorption or emission of radiation.

The matrix-isolation technique, described below, essentially preserves the vibrational and electronic properties of vapor molecules while allowing them to be examined by absorption spectroscopy in their lowest energy levels, a condition that does not occur at their vaporization temperature. Boric oxide and carbon vapors have been successfully investigated by this method.

a. Boric Oxide. The final report on the matrix isolation of B_2O_3 and B_2O_2 in argon and xenon has been prepared and is about to be issued as a Technical Report, which will also contain a brief description of some early work on carbon vapor. The summary of this report is the following:

The matrix isolation technique has been extended to allow molecules which are in equilibrium with solids at high temperatures to be trapped and studied at low temperatures. A beam of the hot vapor issuing from a Knudsen cell or

a heated surface is premixed with a large excess of argon or xenon just prior to condensation at 20°K. The method was applied to boric oxide vapor which was vaporized from the liquid at 1400°K. The infrared absorption spectrum of the B_2O_3 molecule in a solid inert-gas matrix was measured between 280 and 3600 cm^{-1} and compared with the known emission spectrum of the vapor. Several new bands were found near 500 cm^{-1} which led to a considerable alteration in the vibrational assignment and the calculated values of the thermodynamic properties of the gaseous molecule. The infrared spectrum of B_2O_2 (produced by heating boron plus boric oxide) isolated in a matrix yielded one absorption band which agreed with the emission spectrum. A general program is described which was written for the IBM 7090 in order to permit the calculation of molecular force constants from assigned fundamental vibrational frequencies. An extensive normal coordinate treatment of B_2O_3 was made with this program utilizing the observed spectra of B^{10} and B^{11} substituted molecules. The general applicability of the experimental technique is indicated by some preliminary work on the matrix isolation of carbon vapor formed at 2600°K. A strong infrared band appearing at 2040 cm^{-1} is assigned to the C_3 asymmetric stretching frequency. Warming the matrix slightly allowed diffusion of the C_3, C_2 and C species and many new infrared bands appeared. It seems likely that information about the larger molecules in carbon vapor can be obtained in this way.

b. Carbon Vapor. Carbon vapor containing the molecules C_3, C_2, C in the approximate proportions 6:1:2 was produced by inductively heating a rod of spectroscopic-grade graphite to 2400°C.

The matrix isolation of carbon vapor in argon reported in the last Semi-annual Report has now been extended by using neon and xenon matrices. This work has necessarily been carried out at 4°K (liquid helium temperature) since facilities are not yet available for the use of liquid hydrogen in the new Laboratory. It is desirable to measure the spectra of molecules in various matrices in order to learn about the extent of departure from gaseous behavior in such media; this is particularly true of electronic spectra, for which the perturbations are often large.

Figure B-1 shows a comparison of the neon and xenon spectra in the near ultraviolet with the argon result previously reported. The strongest band

occurs at 4226, 4102, and 4054 Å in the xenon, argon, and neon matrices (the spectra were displaced in the Figure in order to show them together), whereas Douglas[6] has found in studies of gaseous C_3 a strong band with a head at 4050 Å which is attributed to a transition between Σ and Π levels. Hence one can see a gradual shift of this band as the molecule is surrounded by the increasingly larger matrix molecules; the red-shifts from the gas value are about 23, 300, and 1030 cm^{-1} in neon, argon, and xenon, respectively. This is qualitatively in accord with a simple theory[7] of the matrix effects on the ground and excited states of the trapped molecule. This theory uses the Lennard-Jones potential function to describe the interaction between the trapped molecule and the rare-gas solid. In this application it gives only poor quantitative agreement with the observed shifts, but it must be said that the simplifying assumptions used in the derivation of the theory must begin to lose their meaning for a relatively large linear molecule such as C_3.

The neon-matrix spectrum is the most promising one for analysis since the perturbations are minimized there. The spectrum should be interpretable in terms of a $\Sigma \longleftarrow \Pi$ or $\Pi \longleftarrow \Sigma$ transition, both of which are consistent with Douglas' analysis. One would expect a $^1\Sigma$ ground state for the C_3 molecule. Since this spectrum was taken at 4°K, the population of any but the lowest vibrational state (assuming no rotation is allowed) of the ground electronic state is very small. The complex nature of the spectrum suggests that interaction of the vibrational and electronic motions (the Renner effect) is occurring in addition to the Fermi resonance that is usually observed in such linear triatomic molecules. The former leads to the appearance of vibronic splittings of bands in the Π state, while the latter causes shifts in the band positions and the appearance of extra bands because of the interaction between the symmetric stretching frequency ν_1, and the first overtone $2\nu_2$ of the bending frequency. An analysis with these complications in mind is now being attempted.

---

(6) A. E. Douglas, Astrophys. J. 114, 466 (1951); K. Clusius and A. E. Douglas Canad. J. Phys. 32, 319 (1954).

(7) M. McCarty, Jr. and G. W. Robinson, Mol. Phys. 2, 415 (1959).

In the infrared spectral region the asymmetric stretching frequency ν_3 in the ground electronic level has been found at 2040 cm^{-1} (see the previous Semiannual Report) in an argon matrix both at 20° and 40°K and occurs unexpectedly as a distinct doublet with a separation of about 4 cm^{-1}. This band has now also been observed in neon and xenon. In neon it also occurs at 2040 cm^{-1} (the matrix was not concentrated enough to establish whether the band is a doublet), whereas in xenon there appear to be two bands at 1993 and 2021 cm^{-1}. The explanation of the splittings is not definitely known; two possibilities are interaction with lattice modes and the existence of sites of slightly different influence on the trapped molecule.

The evidence which has arisen in recent years concerning the ground electronic state of the C_2 molecule and the change of that state in an argon matrix has stimulated renewed interest in its properties. Ballik and Ramsay[8] have established that the ground state of the gaseous C_2 molecule is the $^1\Sigma_g^+$ state and that it lies only 610 $\pm$ 10 cm^{-1} below the $^3\Pi_u$ state. In contrast, Robinson and McCarty[9] have observed that C_2 molecules deposited in a xenon matrix at 4°K yield the Swan bands both in fluorescence and in absorption, which indicates that the $^3\Pi_u$ state lies lower than the $^1\Sigma_g^+$ in this environment. (The Swan bands are a well known system in the gas, there being an observed 0-0 band at 5165 Å and a 1-0 band at 4737 Å for the transition $^3\Pi_g \longleftarrow {}^3\Pi_u$.) Robinson and McCarty prepared their matrices by condensation of the products of a discharge in CH_4, C_2H_2, or isopentane diluted with argon or xenon.

It is clearly of interest to see whether the behavior of C_2 produced by vaporization of carbon will yield the same spectrum. The presence of C_2 in low concentration in comparison with C_3 has meant that only weak spectra have been examined to date. In argon at 20°K an approximate check of the shift of the 0-0 band of McCarty and Robinson is obtained. This is not true for the 1-0 band in argon where these authors find (at 4°K) a vibrational perturbation in

---

(8) E. A. Ballik and D. A. Ramsay, J. Chem. Phys. 31, 1128 (1959).

(9) G. W. Robinson and M. McCarty, the Faraday Society, Informal Discussion on Free Radical Stabilization, Sheffield, Sept. 4-5, 1958

the excited state from 1755 in the gas to 1940 cm^{-1} in the matrix. A similarly derived quantity from our observations leads to a value of 2054 cm^{-1} in the matrix. The present feeling is that both of these assignments are probably incorrect since vibrational shifts (admittedly in the ground electronic state) are usually observed to be small, and almost always occur toward lower frequencies. In xenon at 4°K at least three weak bands are found between 5185 and 5260 Å and two other probable bands at 4692 and 4800 Å. The multiplicity of bands may indicate a poorly prepared matrix, but xenon has caused the appearance of multiple vibrational peaks on other occasions. More experiments are needed to clear up the anomalies observed in the C_2 spectra.

c. Future Work. Preparations are under way for the study of C^{13}-enriched carbon. This should help in unravelling the observations made up to now, particularly in the infrared region. This matrix-isolation technique has been demonstrated to be of general usefulness by the work on B_2O_3 and carbon. It will be available for investigation of the thermodynamic properties of carbides and borides that appear promising in the chemical screening tests.

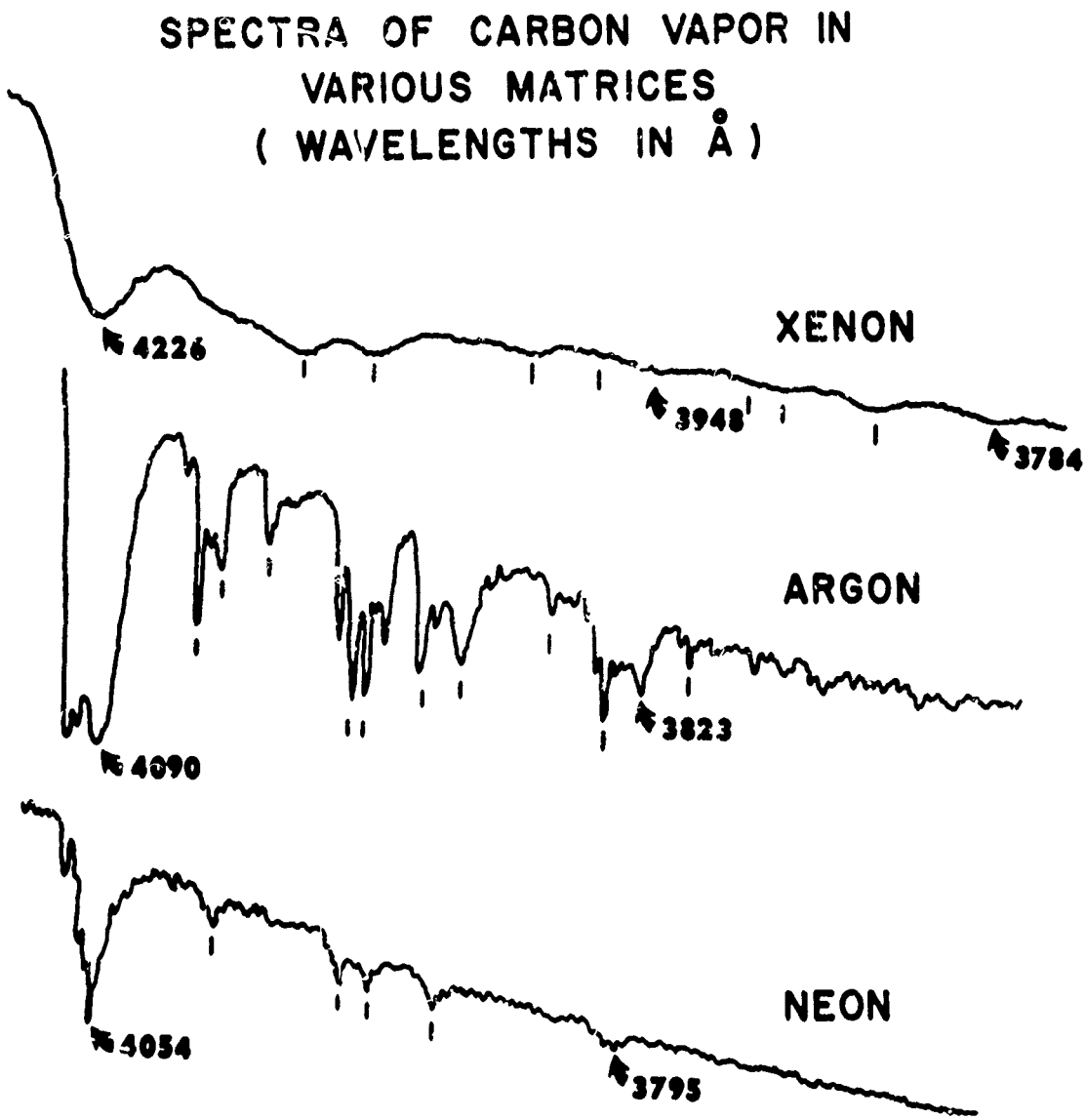
SPECTRA OF CARBON VAPOR IN
VARIOUS MATRICES
(WAVELENGTHS IN Å)
XENON
4226
3948
3784
ARGON
4090
3823
NEON
4054
3795

FIGURE B - 1

C. Elastic Properties

B. T. Bernstein

In the previous Semiannual Report experimental results for the elastic properties of a polycrystalline tungsten sample at temperatures up to 1800°C were reported as well as a broad outline of our research program on elastic properties. An article on these tungsten measurements has been submitted to the Journal of Applied Physics. Because of the extensive use of tungsten for rocket nozzles and also as a consequence of the interesting effects observed during the last period, experimental studies on both monocrystalline and polycrystalline specimens of this metal have been continued. Research on the elastic properties of refractory carbides and borides has been initiated, and preliminary results have been obtained for polycrystalline TiC and for single crystals of TiC and ZrC.

1. Tungsten

Previous dynamic measurements on polycrystalline tungsten showed a smooth decrease with temperature for the shear modulus except in the range of 600-800°C where the decrease was more rapid than above or below this temperature range. The relative attenuation of signal amplitude also showed a similar anomaly and an additional one in the temperature range 650-900°C. Above 1280°C the shear-wave attenuation was so great that measurements could not be made. This behavior was reproduced in several runs with the same sample.

During this period the tungsten sample was annealed at 1800°C for eight hours. Shear-wave measurements made after this treatment showed no change of the damping losses from their previous values. The small attenuation of the compressional-wave amplitude increased smoothly with temperature except in the vicinity of 1800°C where there was a sharper increase. Since this temperature is in the vicinity of the recrystallization temperature of tungsten, this change may have been occurring during the measurements. Two other samples of polycrystalline tungsten that have been machined and annealed at 2200°C for four hours will be studied to check this possibility.

Damping of shear waves may be caused by any one or a combination of factors described by Zener[10] and Niblett and Wilks.[11] The four factors which seem most likely to cause the effects noticed in tungsten are relative motion of the grains of a polycrystalline material at elevated temperatures, stress-induced ordering of interstitial atoms into preferred sites in the body-centered-cubic tungsten lattice, oscillation of dislocations under the influence of an applied stress, and solid-state reactions.

Measurements on single crystals are needed to help determine the mechanisms responsible for the damping in these polycrystalline samples. The absence of grain boundaries should eliminate this factor from consideration. No relaxation as a result of stress-induced ordering should occur along a $< 111 >$ axis in the body-centered cubic lattice, since no interstitial sites become preferred[10] in this direction. Hence any damping along a $< 111 >$ axis of a single crystal should presumably arise from either dislocation motion or solid-state reaction.

Work has been completed on the elastic constants of tungsten single crystals at room temperature. Six Laue x-ray diffraction patterns were taken at random positions on the plane ends of each of three crystals obtained from Linde Company. The cylindrical axis, parallel to which the sonic wave travels, is oriented within 2° of a $< 110 >$ axis of crystal LW-1. Crystals LW-2 and LW-3 show some spread of orientations as a result of lineage structure, but their axes lie within the ranges of 2.3° - 4.1° of a $< 100 >$ axis and 2.0° - 5.1° of a $< 111 >$ axis, respectively. Corrections to the measured ultrasonic sound velocities were computed for these misorientations using the tables of Waterman.[12] Because tungsten is nearly elastically isotropic, these orientation corrections amounted to at most 0.004%, which is negligible compared to the experimental error of 0.02%.

---

(10) C. Zener, Elasticity and Anelasticity of Metals, University of Chicago Press, Chicago, Illinois, 1948.

(11) D. H. Niblett and J. Wilks, Phil. Mag. Suppl., 9, 68 (1960).

(12) P. C. Waterman, Phys. Rev., 113, 1240 (1959).

The values tabulated in Table C-I for the elastic constants of tungsten were computed using the density value of 19.265 g/cm^3 employed by de Klerk and Bolef,[13] whose tungsten crystals were also made by Linde Company. The values which they obtained by a different experimental method are also tabulated in Table C-I, and the agreement is excellent. The anisotropy factor[10] $A = 2C_{44}/(C_{11}-C_{12})$ is computed to be 1.0116 from these data.

Table C-I Elastic Constants of Tungsten at 27°C

Elastic Constants	C_{11}*	C_{12}*	C_{44}*
Present Work	5.2239 ± 0.0017	2.0583 ± 0.0008	1.6011 ± 0.0002
de Klerk and Bolef[13]	5.22	2.06	1.604

* In dynes/cm^2 x 10^{-12}

2. Titanium and Zirconium Carbides

Preliminary results have been obtained on single-crystal TiC and ZrC (Table C-II). These results lead to anisotropy factors $A = 2C_{44}/(C_{11}-C_{12})$ of 0.848 for TiC and 0.756 for ZrC.

Table C-II Elastic Constants of TiC and ZrC at 27°C

Elastic Constant	C_{11}*	C_{12}*	C_{44}*	Assumed Density
TiC	5.245	0.980	1.809	4.906 g/cc
ZrC	4.280	0.408	1.464	6.564 g/cc

* In dynes/cm^2 x 10^{-12}

If the interactions between the atoms of a crystal are described by central forces, if each atom is at a center of symmetry, and if there is no residual stress in the crystal, the well known Cauchy relations between the elastic constants must hold. For cubic crystals the Cauchy relation is

(13) J. de Klerk and D. I. Bolef, Bull. Am. Phys. Soc., 6, 76 (1961).

$C_{12} = C_{44}$. In fact,[14] this relation is not generally satisfied for either metals or non-metals, although it is valid for alkali halides. For metals for which theory shows the valence-electron distribution to be non-localized (Cu, Ag, Au, Al), C_{12} is much greater than C_{44}. For transition metals (Fe, Ni, Mo, W) for which theory shows the d electrons to be localized to some extent, C_{12} and C_{44} are closer in value. In contrast, TiC and ZrC, like C, Si, and Ge, have $C_{44} > C_{12}$, although the transport properties of these carbides are typical of metals. This combination of properties might be produced by strongly localized d orbitals between the metal and carbon atoms, resulting in highly directional lattice forces, and by non-localized s electrons giving rise to the metallic transport properties. Such an interpretation is in accord with the galvanomagnetic measurements reported in Section E.

An interesting point of comparison with the parent metals can be expressed in terms of the Debye temperatures. The Debye temperatures of TiC and ZrC, calculated from the data in Table C-II, are compared with those for Ti and Zr in Table C-III. It is seen that the addition of carbon to titanium and zirconium to form TiC and ZrC greatly changes the lattice vibrational properties of these elements.

Table C-III Debye Temperatures of Ti, Zr, TiC, and ZrC

Metal	ΘD (°K)
Ti	380
TiC	734
Zr	250
ZrC	529

A sample of titanium carbide powder was hot pressed at 2300°C to a measured density of 4.21 g/cc. This powder, Lot No. C-29, was reported to be $TiC_{.97}$ with 2% impurities, principally nitrogen and free carbon. The elastic properties of the sample, calculated from measurements of ultrasonic velocities

(14) H. B. Huntington, Solid State Physics, edited by F. Seitz and D. Turnbull, (Academic Press, Inc., New York, 1958) Vol. 7 pp. 213-351.

and density, are shown in Table C-IV, as are the results of Spinner[15] for a sample of 3.56 g/cc density. In addition, elastic constants computed for an idealized polycrystalline material from the data on monocrystalline TiC are included in Table C-IV. Voight's formulas[14] or $E = (C_{11}-C_{12} + 3C_{44})(C_{11} + 2C_{12})/(2C_{11} + 3C_{12} + C_{44})$, $\mu = (C_{11} - C_{12} + 3C_{44})/5$, and $K = 3/(C_{11} + 2C_{12})$ were used to compute Young's modulus, the shear modulus, and the compressibility, respectively. Poisson's ratio changes very little with density, but the elastic moduli decrease as the porosity increases. Theoretical treatments have been made of the effects of porosity on elastic properties, for example by MacKenzie[16] for spherical pores. However, the results are sensitive to the form and distribution of the pores and so cannot be universally applied.

Table C-IV Elastic Moduli of Polycrystalline TiC

Sample	Density*	Young's** Modulus	Shear** Modulus	Poisson's Ratio	Compressibility***
Averaged Single Crystal	4.906	4.582	1.938	0.182	4.163
Hot Pressed	4.21	2.687	1.132	0.187	6.989
Spinner[15]	3.56	1.774	0.7489	0.189	10.68

* g/cc

** units of 10^{12} dynes/cm^2

*** units of 10^{-13} cm^2/dynes

3. Pyrolytic Graphite

The room-temperature dynamic elastic properties of pyrolytic graphite have been measured at a 10-megacycle frequency by an ultrasonic pulse technique. In certain directions of wave propagation the attenuation is small enough for the pulse technique to be applicable. In contrast, this technique cannot be used for most polycrystalline graphites because of the large effective acoustical attenuation at this frequency. Three specimens of pyrolytic graphite from the National Carbon Research Laboratories were measured, and the

(15) S. Spinner, J. Res. NBS 65C, 89 (1961).

(16) J. K. MacKenzie, Proc. Phys. Soc., (London) 63B, 2 (1950).

velocities of propagation are given in Table C-V. It was not possible to transmit a measurable ultrasonic pulse for transverse waves in the layered planes.

Assuming that the individual crystallites have their basal planes parallel to the layered planes some of the dynamic elastic constants can be derived from the velocity data in Table C-V.

Table C-V Ultrasonic Velocities in Pyrolytic Graphite (27°C)

Direction of Propagation	Mode of Vibration	Velocity ($cm\ sec^{-1}$)
Perpendicular to layered planes	longitudinal	3.68×10^5
	transverse	0.960×10^5
Parallel to layered planes	longitudinal	6.13×10^5
	transverse - parallel	attenuation prevented measurement.
	transverse - perpendicular	

The elastic constants found are compared in Table C-VI with the predicted values of Bowman and Krumhansl[17] and a measured value by Bacon[18] for a graphite whisker.

Table C-VI Elastic Constants of Graphite in Units of 10^{11} dynes/cm^2

Elastic Constant	Present* Work	Bowman and Krumhansl	Bacon
C_{11}	8.19	113.0	70.0
C_{33}	2.95	> 1.8	----
C_{44}	0.201	0.23	----
C_{12}	-----	25.0	----
C_{13}	-----	-----	----

* A measured density of 2.18 g/cc was used in calculating the elastic constants.

(17) J. C. Bowman and J. A. Krumhansl, J. Phys. Chem. Solids, 6, 367 (1958).

(18) R. Bacon, J. Appl. Phys., 31, 283 (1960).

It is interesting to note that C_{11}, derived from the measured longitudinal velocity in the layered planes, is an order of magnitude smaller than the values quoted by Bacon[18] and by Bowman and Krumhansl.[17] Since the velocity of this wave is independent of the direction in the basal plane of a hexagonal crystal, it is not very reasonable to explain the disagreement on the basis of azimuthal misorientations of the planes. On the other hand, the presence of voids and pores in the layered plane could greatly reduce the elastic constant, as shown by MacKenzie.[16] The result that C_{33} and C_{44} are roughly in agreement with the predicted values of Bowman and Krumhansl lends support to this interpretation, since the presence of defects in the layered planes should not strongly affect the velocity of waves travelling perpendicular to this plane.

4. Future Plans

In continuing this work the dynamic elastic properties of both monocrystalline and polycrystalline samples of TiC and ZrC will be measured at elevated temperatures. Research will be continued on the elastic properties of single-crystal tungsten to high temperatures to investigate the damping found in polycrystalline material at 1280°C and above. The effect of recrystallization on the elastic behavior of polycrystalline tungsten will be studied with samples annealed at 2000°C.

These measurements can be extended above 1800°C by a new resistance-heated furnace which is complete except for fabrication of a few heater-element parts. As dicusssed in carlier reports, elastic-loss determinations are a sensitive measure of the effect of structural imperfection upon the mechanical properties of materials and are important both for characterizing the materials and for understanding mechanisms of atomic and dislocation movement. As a consequence, plans are under way to construct experimental equipment for quantitative measurement of elastic loss over a wide range of temperatures and stress frequencies. Measurements at liquid helium temperatures, as well as at high temperatures, are needed in order to obtain a more complete picture of the temperature dependence of elastic moduli and elastic losses.

D. High-Temperature X-Ray Studies

C. R. Houska

An increase in temperature produces two related changes in an atomic lattice. The atoms vibrate with increased amplitude, and the lattice expands. X-ray diffraction techniques are currently being used to determine these changes as functions of temperature for titanium and zirconium carbides. The lattice expansion, so important in determining thermal stresses in composite or unevenly heated bodies, is determined directly from the change in lattice parameter with temperature. The mean atomic vibration amplitudes can be obtained from data on the integrated intensities of several diffraction lines as functions of temperature.

Refractory compounds such as TiC, ZrC, TiN, and ZrN have the NaCl structure and follow the empirical atomic-size rule first recognized by Hägg. The rule states that when the ratio of interstitial atomic diameter to that of the metal atomic diameter is less than about 0.59, simple crystal structures are found. An additional condition is that the ratio have a lower limit of 0.41, at which value the interstitial atoms in octahedral sites in a FCC lattice just make contact with the metal atoms. ZrC (0.48) and TiC (0.52) follow this rule, as do ZrN (0.44) and TiN (0.48).[19]

In general each atomic species in a lattice may have a different mean vibration amplitude. However, in view of their tight packing and high melting points one might question the possibility of unequal magnitudes of vibration in these carbides. Determinations of the atomic vibration amplitudes in carbides will give added insight into the behavior of interstitial compounds.

1. Thermal Expansion

The thermal expansion of titanium carbide was measured from x-ray diffraction-line shifts using the same furnace discussed in previous reports. Data were obtained using the $\begin{pmatrix} 511 \\ 333 \end{pmatrix}$ and (422) lines and the procedure of Mauer and Bolz.[20]

---

(19) Schwartzkopf, P., and Kieffer, R., Refractory Hard Metals, Macmillan Co., N. Y. (1953).

(20) Mauer, F. A., and Bolz, L. H., "Measurement of Thermal Expansion of Cermet Components of High Temperature X-Ray Diffraction", Nat. Bur. Stds., Dec. 1955, ASTIA No. AD95329.

This requires that the lattice parameter from two lines be identical, and it thereby corrects for small shifts of the specimen surface. Three specimens prepared by identical powder metallurgical techniques were used for the measurements. The expansion data are given in Table D-I along with the best available published data.(21)

Table D-I Thermal Expansion of TiC

Temperature	(°C)	25	500	750	1000	1250	1500	1700
Expansion	(%)	0	.31	.54	.86	1.14	1.39	1.65
Literature	(%)	0	.32	.52	.76	1.06	1.40	-

Temperature was measured by sighting into a nearly black-body hole with a length-to-diameter ratio of 6/1. The bottom of the hole was within 1/16" of the diffraction surface. The present measurements extended published expansion data by about 200°C. Higher temperatures are expected to be attained with a new hot-zone assembly of improved design that has recently been completed.

2. Vibration Amplitudes for TiC

The integrated x-ray line intensities from TiC powders can be represented by $I(T,hkl) \approx (LP)\, j \left[f_{Ti} \exp(-M_{Ti}) \pm f_C \exp(-M_C) \right]^2$, (1)

where + and - refer to the cases of all even or all odd hkl, LP is the Lorentz and polarization factor, j is the multiplicity, and f_{Ti} and f_C are the atomic scattering factors for Ti and C. M_x is defined by $M_x = \frac{8}{3}\pi^2 \langle \mu_x(T)^2 \rangle \frac{\sin^2\theta}{\lambda^2}$, θ being the Bragg angle, λ the x-ray wavelength, and $\mu_x(T)$ the root-mean-square amplitude of vibration of species x.

From Figure D-1 it is seen that the experimental intensities lie within experimental error of the curves calculated on the assumption that the mean vibration amplitudes of the titanium and the carbon atoms are equal. When this is true, as it appears to be here, Equation (1) can be simplified to

$$I(T,hkl) \approx LPj \exp(-2M) (f_{Ti} \pm f_C)^2; \quad (2)$$

therefore,

$$\exp -2 \left[M(T) - M(RT) \right] = \frac{C(T,hkl)}{C(RT,hkl)} \quad (3)$$

(21) Goldsmith, A., Waterman, T. E., Hirschhorn, H. J., Handbook of Thermophysical Properties of Solid Materials, Vol 4, Macmillan Co., N. Y. (1961).

where

$$C(T,hkl) = \frac{I(T,hkl)}{LPj(f_{Ti} \pm f_C)^2}$$

Figure D-2 illustrates the values of $\frac{16}{3}\pi^2\left[\langle u(T,hkl)^2\rangle - \langle \mu(RT,hkl)^2\rangle\right]$ for each diffraction line as a function of temperature. All the lines appear to fall on the same curve within the experimental error. The 1700°C data show considerable scatter which probably results from grain growth in the specimen.

The root-mean-square vibration amplitudes of the atoms in TiC, calculated from the experimental data, are presented in Table D-II.

Table D-II RMS Vibration Amplitude in TiC

Temperature (°C)	25	500	750	1000	1250	1500	1700
$\langle \mu^2 \rangle^{1/2}$ (Å)	0.096	0.151	0.171	0.183	0.216	0.242	0.279

The Debye temperature Θ varies with temperature as discussed in the previous Semiannual Report (p. 62). A series of Debye temperatures were calculated from the data of Figure D-2, using an approach devised by Chipman.[22] These are listed in Table D-III.

Table D-III Debye Temperatures for TiC vs Temperature

Sample Temperature (°C)	25	500	750	1000	1250	1500	1700
Debye Temperature (°K)	730	710	712	740	689	660	604

In using the Debye formulation for vibration amplitudes, an average mass was used. This assumes an artificial monatomic solid in which all atoms of the NaCl lattice have the same average mass $\bar{m}$, as has been done by Lonsdale.[23]

3. Future Plans

During the next quarter measurements will be made on TiC, ZrC, TiN, and ZrN. In addition, attention will be paid to the effects of varying the metal: metalloid ratio. Reducing the carbon or nitrogen content would be expected to influence both the thermal expansion and the vibrational amplitudes, as well as other physical properties.

---

(22) Chipman, D. R., Journal of Applied Physics, 31, 2012 (1960).

(23) Lonsdale, K., Acta Cryst., 1, 142 (1948).

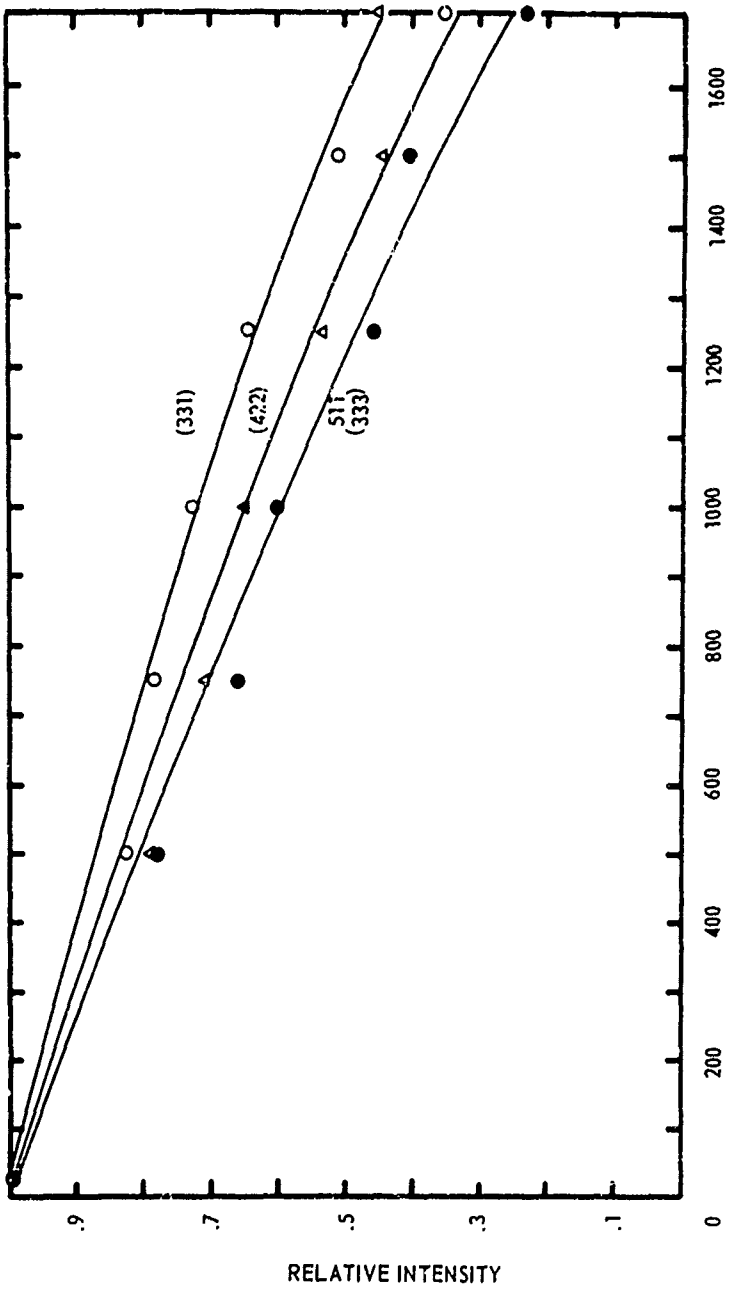

FIGURE D - 1. INTEGRATED INTENSITY DATA FOR TiC NORMALIZED AT 25°C.
SOLID CURVES CALCULATED FROM AVERAGE OF FIG. D - 2.

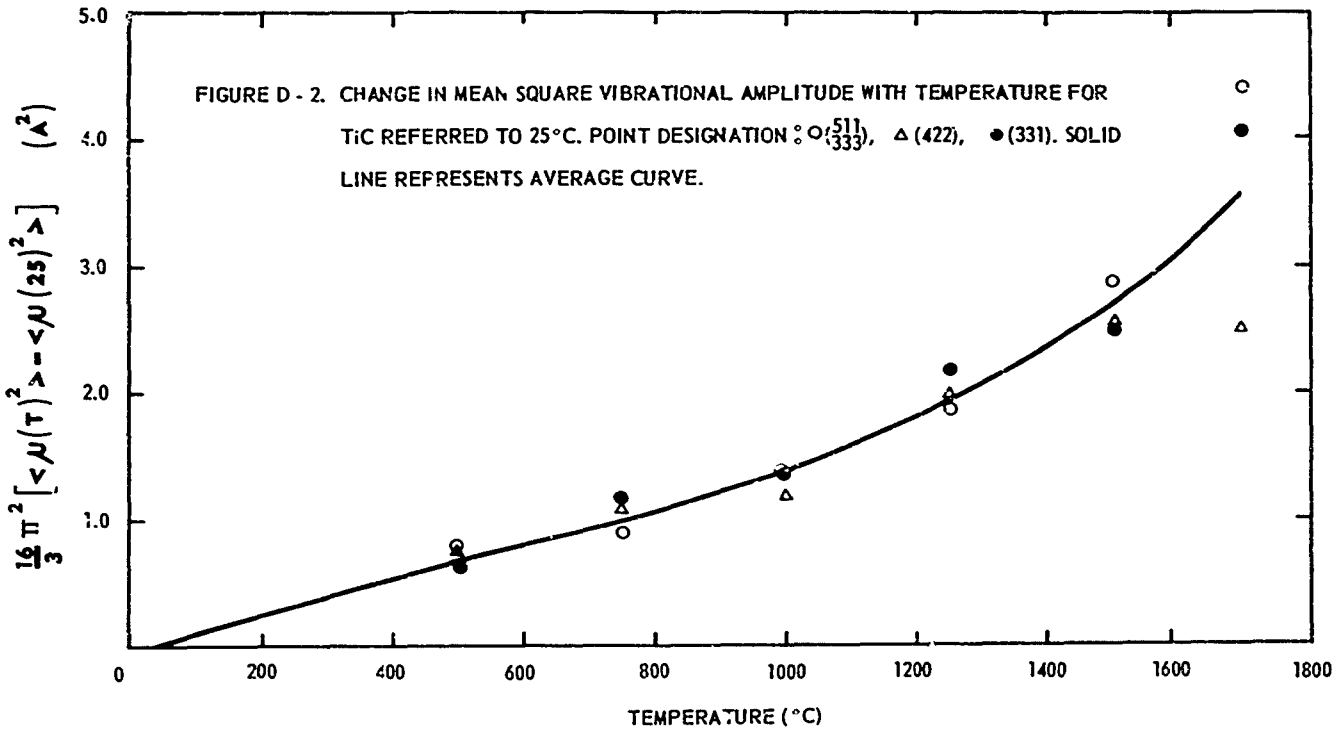

FIGURE D - 2. CHANGE IN MEAN SQUARE VIBRATIONAL AMPLITUDE WITH TEMPERATURE FOR TiC REFERRED TO 25°C. POINT DESIGNATION ○ ○ $(\frac{511}{333})$, △ (422), ● (331). SOLID LINE REFRESENTS AVERAGE CURVE.

E. Galvanomagnetic Measurements

The present study of the galvanomagnetic effects in refractory carbides and borides has three principal objectives: to obtain a qualitative understanding of the behavior of the valence electrons in these materials, to provide experimental information which will aid in the formulation and evaluation of applicable theoretical calculations concerning the chemical bonding, and to aid in the characterization of samples with regard to such factors as composition, grain-boundary effects, and porosity. The galvanomagnetic effects will parallel changes in other physical properties related to chemical bonding, such as hardness and brittleness; and a knowledge of these effects will aid in determining compositions which optimize desirable physical characteristics.

1. Equipment

The electronic equipment for measuring resistivity, Hall effect, and magnetoresistivity is in operation and has proved to be entirely satisfactory. The measurement circuit used is given in Figure E-1 and follows the general design of Donaghue and Eatherly.[24] With the exception of the phase shifter, all components are standard commercial instruments, and very little special electrical shielding has been necessary. The Hewlett-Packard wave analyzer has an oscillator output and thus acts as both an a.c. source and a narrow-band voltmeter inherently tuned to the same frequency. The power amplifier is necessary to provide sufficient current for measurements on the refractory carbides and borides. The current that generates the resistive or Hall potential also powers the calibrated voltage divider which in turn "bucks" the potential from the sample and, by adjustment to make the signal to the strip recorder a minimum, is used to measure the output from the Hall or resistance probes. Both measurements can be made on the same sample using three voltage probes and a simple switching arrangement. With this technique the measurements are not sensitive to fluctuation of the primary current

---

(24) J. J. Donaghue and W. P. Eatherly, Rev. Sci. Instr. 22, 513, (1951).

through the sample. The wave analyzer and preamplifier are capable of readily detecting imbalances of 0.01 microvolt between the outputs of the voltage divider and the sample, with a time constant of the order of two seconds. The use of alternating current makes the measuring circuit insentive to thermoelectric and thermomagnetic effects. This attribute has proved valuable by permitting measurements to be made rapidly as a function of temperature without elaborate temperature control.

A double Dewar system and cell for measurements from 4.2°K to room temperature are in operation. A furnace for high-temperature measurements is being designed but is not yet complete. A 12-inch Varian electromagnet provides magnetic fields up to 12 kilogauss for measurements with the liquid helium equipment or a furnace, and to 18 kilogauss for measurements from liquid-nitrogen to room temperatures. New pole pieces to provide 35 kilogauss for measurements near room temperature are being constructed.

2. Titanium and Zirconium Carbides

Titanium carbide has been studied in most detail since single crystals were available. The single crystals, supplied by Linde Company, were nonstoichiometric with an approximate composition of $TiC_{0.94}$. For these measurements the magnetic field, current, and Hall voltage were aligned in the < 100 > directions of the NaCl-type crystals. The temperature dependence of the resistivity ρ and the Hall coefficient R for one crystal are given in Figure E-2. A second sample, cut from a different single crystal, showed approximately the same temperature dependence. Measurements were made at 4.2°K and continuously from 77° to 313°K, with an uncertainty in the temperature dependence as indicated by the widths of the curves in Figure E-2. Values of R and ρ for two single crystals (designated I and II) and an 85% dense hot-pressed TiC sample prepared from single crystal material are given in Table E-I. The chief uncertainties are in the values of the sample dimensions and of the orientation of the magnetic field. No magnetic-field dependence (less than 1%) of R was observed at 4.2°K for field changes from 1 - 12 kilogauss.

Table E-I The Resistivity and Hall Coefficient of Some TiC Samples

	Monocrystalline		Polycrystalline
Resistivity (microhm-cm)	I	II	
300°K	178 ± 8	170 ± 8	90 ± 4
77°K	154 ± 7	143 ± 7	71 ± 4
Hall coefficient (cm^3/coul x 10^4)			
300°K	-14.1 ± 0.4	-13.7 ± 0.4	- 9.0 ± 0.3
77°K	-24.8 ± 0.8	-27.6 ± 0.8	-16.4 ± 0.6

At 77°K the resistivity of the single crystals increased of the order of 5 parts in 10^5 when the field was increased from zero to 17 kilogauss. This increase in ρ appeared to have a quadratic field dependence. The resistance change is very small, however, and the data can only be regarded as qualitative.

The measurements on the hot-pressed TiC sample are in accord with the single-crystal results. The Hall coefficient, while smaller than the single crystal values because of sample porosity, shows an identical temperature dependence. This indicates that profitable work may be performed on hot-pressed samples when single crystals are not available. The broad composition range available in hot-pressed samples should be most useful.

The large change in the resistivity of the single-crystal material upon crushing and hot-pressing is very interesting. It is doubtful that sufficient impurities were introduced during crushing to account for the change, although relief of strains or increase in the C-to-Ti ratio during hot-pressing in a graphite mold may not be ruled out. While further work is needed to establish the cause of the change, the effect indicates the sensitivity of the measurements to sample history and their usefulness for characterization of materials.

Initial measurements on hot-pressed ZrC give values of 58.8 and 46.8 μohm-cm for the resistivity at 300°K and 77°K, respectively.

3. Future Plans

Measurements on monocrystalline ZrC and on polycrystalline ZrC and ZrC/TiC solid solutions are in progress to reveal the effect of changing the period of the metal. The difference in resistivity between the single crystal and hot-pressed carbide requires further work on both structures to establish its causes.

A tentative band model for TiC is being considered to suggest the direction of future work. Replacement of some of the carbon with boron or nitrogen should produce considerable changes in the temperature dependence of the Hall coefficient. Measurements on suitable hot-pressed samples should, therefore, provide significant information concerning the role of the interstitial in these materials.

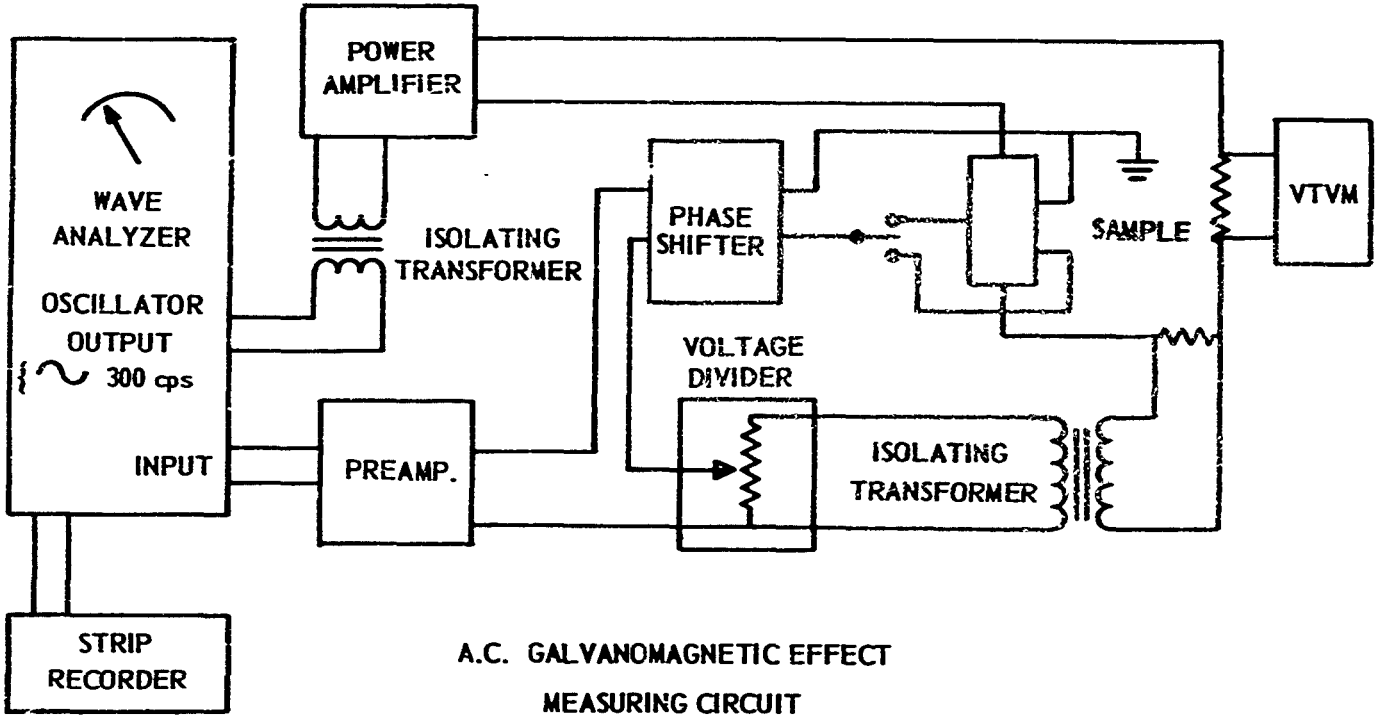

A.C. GALVANOMAGNETIC EFFECT
MEASURING CIRCUIT

FIGURE E - 1

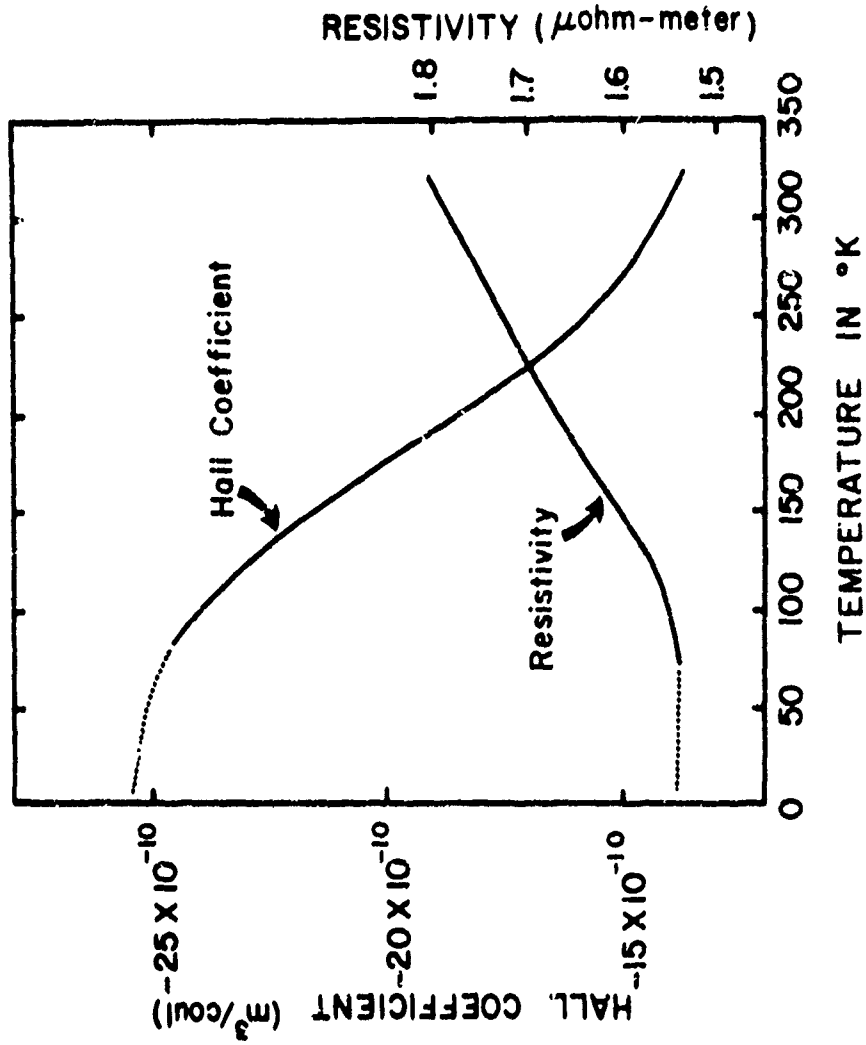
RESISTIVITY (μohm-meter)
1.8
1.7
1.6
1.5
350
300
250
200
150
100
50
0
TEMPERATURE IN °K
Hall Coefficient
Resistivity
HALL COEFFICIENT (m³/coul)
-25 X 10⁻¹⁰
-20 X 10⁻¹⁰
-15 X 10⁻¹⁰

FIGURE E - 2

A major objective of this work is to provide reproducible, characterized specimens of refractory carbides and borides in a variety of shapes, as required for various measurements. For this reason batches of the compounds listed in Table F-I have been prepared. The powders which have been hot-pressed (without binders) into specimens for investigation are given in Table F-II. In addition to specimen preparation, a study of the purification of TiC, ZrC, TiB_2, and ZrB_2 powders and samples by heating them in a vacuum furnace has been started. Specifications for induction-heated equipment in which electrically conducting materials can be zone melted, drip melted, levitation melted, or zone sintered have been prepared, and the equipment ordered from the Lepel Company.

Table F-I Refractory-Compound Powders Prepared

TiC	TiB_2	VC	VB_2	CrB
ZrC	ZrB_2	CbC	CbB_2	Mo_2B
HfC	HfB_2	TaC	TaB_2	LaB_6
		Ta_2C		

Table F-II Hot-Pressed Polycrystalline Specimens

Material	Maximum Density Obtained	Material	Maximum Density Obtained
TiC	95%	TiB_2	92%
ZrC	99%	ZrB_2	95%
HfC	92%	TaB_2	90%
TaC	85%	NbB_2	90%
CbC	85%	LaB_6	92%

1. Preparation of Carbides

Most of the materials-preparation work during this period has had to do with the FCC monocarbides of the 4th and 5th Group transition metals. The carbides are prepared by reaction under purified hydrogen of powders of graphite and the appropriate metal hydride, metal, or metal oxide. In some instances, TaC and CbC for example, the above procedures carried out with

scrupulous care in all details gives directly a product of very good purity. In other cases, however, the results are less favorable, and a vacuum purification step has been found desirable. This treatment consists of heating the crushed raw product in a tungsten container under a vacuum of about 5×10^{-5} mm Hg. A brightness temperature of 2000° - 2200°C, read on the loosely fitting tungsten crucible cover, is attained, with pauses at temperatures where gas evolution occurs. The actual temperature of the charge is estimated to be about 150° - 250°C above the brightness temperature as a result of corrections for sight glasses, prism, and emissivity.

Chemical analyses have been made of the powders prepared, and typical composition data for the carbides prepared by solid-state reactions are given in Table F-III. These analyses all refer to fine powders, minus 200 mesh or finer, ready for further processing by powder metallurgical techniques. In the carbides the metal-plus-carbon content is reported considering only the combined carbon; free carbon is considered as an impurity. Oxygen analyses have been done by Ledoux Company with a Leco conductometric analyzer. In addition, spectrochemical analyses have been made for trace elements such as aluminum and chromium.

Table F-III Refractory Compound Analyses

ZrC Lots (Weight %)

Lot No.	O	N	Fe	Si	Free C	Comb. C	Zr + Comb. C	Comb. C/Zr*
Theoretical	0	0	0	0	0	11.63	100	1.00
C-12	-	0.59	0.08	-	0.77	11.21	98.83	0.97
V-10**	0.25	0.34	0.03	< 0.05	0.81	10.79	98.24	0.94
C-20	0.47	0.27	0.14	< 0.05	0.41	10.89	98.23	0.95
V-13**	0.065	0.28	< 0.05	< 0.05	< 0.05	11.22	99.70	0.965
C-21	0.32	0.35	0.14	< 0.05	0.37	11.04	99.08	0.955
C-31	0.30	0.06	0.05	< 0.01	0.82	10.75	98.98	0.925

* Atomic ratio of combined carbon to zirconium.

** Lots V-10 and V-13 were produced by vacuum purification of Lots C-12 and C-20 respectively at about 2000° C for approximately one hour.

Table F-III Refractory Compound Analyses

TiC Lots (Weight %)

Lot No.	O	N	Fe	Si	Free C	Comb. C	Ti + Comb. C	Comb. C/Ti*
Theoretical	0	0	0	0	0	20.	100	1.00
C-13	-	1.00	0.19	-	0.60	18.78	97.5	0.955
C-22	-	0.82	0.23	0.03	0.50	-	-	0.94
V-17**	0.061	0.80	0.15	< 0.05	0.28	19.01	98.45	0.96
C-29	-	0.41	0.11	-	0.73	19.06	98.0	0.965
C-30	0.22	0.62	0.11	-	0.83	18.80	98.2	0.95
V-34**	0.072	0.27	0.01	-	0.60	18.82	98.25	0.955

* Atomic ratio of combined carbon to titenium.

** Lot No. V-17 was produced by vacuum purification from C-22, Lot No. V-34 from a very impure early batch. V-17 was heated to 1920°C for 10 minutes and V-34 to 2050°C for 30 minutes.

Table F-III Refractory Compound Analyses

Miscellaneous Carbides (Weight %)

Lot No.	Cpd.	O	N	Fe	Free C	Comb.* C	Metal + Comb. C	Comb. C/Metal**
C-24	TaC	0.020	0.01	0.03	0.10	6.12	99.6	0.99
C-25	CbC	0.048	0.04	0.06	0.11	11.10	99.45	0.985
C-36	CbC	-	0.03	0.11	0.36	11.21	98.7	0.995
C-17	HfC	-	0.80	0.01	0.52	5.43	98.4	0.85
C-19	HfC	0.076	0.59	0.01	1.55	5.51	97.5	0.87
V-12***	HfC	-	0.34	0.05	1.21	6.24	98.5	0.98

* The theoretical combined carbon percentages are TaC - 6.22%, CbC - 11.43%, and HfC - 6.36% to 6.42% depending on Zr content.

** Atomic ratio of combined carbon to Ta, Cb, or Hf.

*** Lot No. V-12 produced from C-19 by vacuum purification.

Among the ZrC lots are two, V-10 and V-13, that were produced by vacuum purification. V-10 was an early run in which the heating was relatively rapid.

Some purification was accomplished, but the amount is lost in analytical discrepancies. Lot V-13 was heated with pauses to 2020°C where it was held for one hour. Considerable purification, especially from oxygen and free carbon, was obtained. It is believed that this purity can be duplicated regularly.

The purities reported for TiC powders are not as good as those for ZrC. The raw carbide has not been produced with as high purity, and analytical results are only available for vacuum purification treatments run at relatively low temperatures (V-17) or on a very impure material (V-34).

Both TaC and CbC have been produced directly with high purity and an excellent approach to the stoichiometric composition. The batches of HfC, made from HfO_2, are not nearly so good, but they compare well with TiC and ZrC. Vacuum treatment of the HfC appears to decrease the nitrogen content and increase markedly the combined-carbon content.

X-ray diffraction is also used to characterize these compounds. It is a relatively sensitive tool for detecting other phases, and it has never revealed a second phase in our materials other than graphite in a few cases and the expected V_2C in a VC batch markedly low in carbon. Determination of lattice parameter should reveal differences in composition. For these carbides and borides, unfortunately, there exist no standard values of lattice parameter determined from high purity samples of known composition. The lattice parameters reported for ZrC in the past fifteen years range from 4.678 - 4.695 Å. Our materials (Table F-IV) lie at the top of that range, 4.695 - 4.697 Å. As Hansen[25] states, this is probably the correct value for stoichiometric ZrC, since a carbon deficiency would be expected to decrease the lattice constant. The lattice parameters of our TiC likewise lie within and near the top of recent literature values. TaC and CbC also agree in lattice parameter with published data. HfC has a smaller parameter than

---

(25) M. Hansen and K. Anderko, Constitution of Binary Alloys, McGraw-Hill, (1958).

reported elsewhere, but the zirconium contents of the materials differ, 2-3% for our material vs 4-5% for the other. The shape of the diffraction line can also be informative. If the specimen material is nonhomogeneous, a broadening of the diffraction line occurs. This has been found in a number of instances as noted in Table F-IV. Vacuum treatments eliminate this nonhomogeneity in ZrC and TiC.

Table F-IV X-ray Measurements

Material	Lot No.	Lattice Parameter (Å)	Literature*	Line Shape
ZrC	C-12	4.695	4.678-4.695	Prominent high-angle tailing
ZrC	V-10	4.696		Symmetrical
ZrC	V-13	4.697		Symmetrical
ZrC	C-31	4.697		Symmetrical
TiC	C-13	4.327	4.313-4.329	Distinct high-angle tailing
TiC	C-30	4.327		Some high-angle tailing
TiC	V-17	4.323		Symmetrical
TaC	C-24	4.456	4.456	Symmetrical
CbC	C-25	4.470	4.450-4.487	Symmetrical
HfC	C-19	4.629	4.640-4.646	Symmetrical
HfC	V-12	4.633	4.640-4.646	Symmetrical

* The TaC value is for $TaC_{0.91}$; the HfC values are for material containing 4-5% Zr, compared to 2-3% in the present material.

2. Preparation of Borides

A summary of the analytical data obtained on various refractory borides is given in Tables F-V, F-VI, and F-VII. These borides were prepared by the reaction of boron with metal, metal-hydride, or metal-oxide powders under a purified hydrogen atmosphere. In general the analyses obtained on the borides do not appear to be of high accuracy. Discrepancies between total analyses and

100% often exceed 2%, despite analysis for a wide range of materials, including all elements that could reasonably be expected to exist in these borides in amounts greater than a few parts per million. The results of the vacuum purification treatments indicate that large decreases in the nitrogen, oxygen, and carbon contents can be produced.

3. Future Work

During this period samples for gas-solid reactions, x-ray studies, galvanomagnetic measurements, and elasticity determinations have been made by hot-pressing techniques. This work will be continued and extended to larger samples for thermal-property and mechanical-property measurements.

Specially designed Lepel equipment that uses induction heating for drip melting, moving-zone melting, moving-zone sintering, and levitation melting in a vacuum or inert atmosphere has been ordered. However, it will not be delivered during the coming quarter. Work on vacuum purification of carbides and borides will be continued in the coming months.

TABLE F-V - Analyses of ZrB_2 Lots (Wt. %)

Lot*	Zr	B	B/Zr**	B + Zr	C	N	O	Fe	Total
B-2	78.84	18.81	2.01	97.65	0.54	0.35		0.31	98.90 + O_2
B-6	78.06	19.37	2.08	97.43	0.65	0.67	0.29	0.20	99.31
B-13	77.35	18.71	2.04	96.06	0.91	0.72	0.64	0.20	98.62
B-19	77.07	19.61	2.14	96.78	0.61	1.03		0.09	98.56 + O_2
V-25	78.43	19.81	2.13	98.34	0.47	1.10		0.13	99.12 + O_2
B-24	80.05	17.75	1.87	97.95	0.24	0.08		0.10	98.7 + O_2
V-24	80.77	17.78	1.86	98.71	0.05	<0.05		0.05	98.7 + O_2
B-36	78.48	18.50	1.99	97.15	0.93	0.01		0.16	98.3 + O_2
V-32	78.74	19.29	2.06	98.19	0.81	21 ppm	0.07	.15	99.3
B-43	78.95	18.38	1.96	97.37	1.10	53 ppm	0.13	0.16	98.7
V-44	---	---	---	---	---	---	0.02		

* Vacuum-purified lots (V) follow immediately the material from which they were produced.

** Atomic ratio of boron to zirconium.

TABLE F-VI - Analyses of TiB_2 Lots (Wt. %)

Lot*	Ti	B	B/Ti**	B + Ti	C	N	O	Fe	Total
B-38	66.39	31.96	1.81	98.11	1.02	0.07	0.64	0.27	100.45
B-34	63.72	28.15	1.95	91.88	1.61	1.77		0.24	95.7 + O_2
V-29	67.16	30.34	2.00	97.55	0.63	0.12		0.10	98.5 + O_2
B-21	65.54	30.36	2.04	95.90	0.35	0.34		0.09	96.7 + O_2
V-18	66.27	31.97	2.14	98.24	0.24	< 0.05		0.08	98.6 + O_2
B-20A	63.41	30.64	2.14	94.05	1.35	1.07		0.14	96.6 + O_2
V-15	66.20	31.62	2.11	97.82	0.87	0.04		0.11	98.9 + O_2

* Vacuum-purified lots (V) follow immediately the material from which they were produced.

** Atomic ratio of boron to titanium.

TABLE F-VII - Analyses of Miscellaneous Boride Lots (Wt. %)

Material	Main Metal	B	B/Me*	B + Me	C	N	O	Fe	Total
CrB	81.39	16.79	0.99	98.18	0.17	0.22	0.23	0.04	99.0
MO_2B	93.17	5.93	0.56	98.50	0.72	0.04	1.21	0.20	100.7
CbB_2	79.87	18.41	1.98	98.46	0.11	<0.05	0.35	0.12	99.15
TaB_2	88.80	10.08	1.90	98.9	0.14	0.04	0.11	0.08	99.3
TaB_2	87.77	11.16	2.12	98.93	0.07	<0.01	0.077	0.16	99.3
HfB_2	84.48	10.94	2.02	98.32	0.19	0.37	--	0.25	99.13 + O_2
HfB_2	82.32	12.98	2.44	98.64	0.60	0.41	0.10	0.30	100.06
HfB_2(V)	82.90	12.72	2.40	98.71	0.56	0.03	--	0.09	99.55 + O_2

* Atomic ratio of boron to main metal.

G. Mechanical Properties at High Temperatures

1. Creep of Refractory Materials

F. G. Keihn

The mechanical properties of rocket-nozzle materials are very important since the nozzles are subjected to considerable loads and to high thermal stresses during operation. Since the ability to deform plastically and so reduce stress concentrations is vital in such service, the plastic behavior of refractory carbides and borides at high temperatures is particularly important to ascertain.

The construction of a furnace and the acquisition of a tensile creep machine have been reported previously. This furnace and loading system have been very satisfactorily aligned by the use of strain gages on a dummy specimen so that the bending moment on the specimen is minimized. In Figure G-1 is shown a comparison of the bending load, expressed as percent of the tensile load, for a typical commercial machine, for the special axial-loading machine of Jones and Brown,[26] and for our equipment.

A prototype steel specimen has been loaded at 800°C in the equipment and the creep strain measured optically. Tantalum samples and grips have now been machined, and testing near 1400°C is about to begin. Several changes have been made to prepare the equipment for this testing. Brazed water-cooled pull rods have had to be replaced with welded rods to prevent the development of leaks during creep testing. The furnace element has been redesigned for longer life. The temperature controller, which was delivered with some faulty connections, has been repaired.

In the tests on tantalum, and subsequently on refractory carbides and borides, creep strength and ductility will be determined as functions of stress and temperature. In addition, activation energies will be obtained from tests

---

(26) M. H. Jones and W. F. Brown, Jr., ASTM Bull. 1956 pp. 53-59.

in which the temperature is rapidly changed. It is hoped that a unique activation energy, perhaps corresponding to the activation energy for diffusion of one of the constituents, will be found. Specimens of commercial titanium diboride have been obtained from the National Carbon Company, and these will be tested after the tantalum.

2. Lattice Defects and Mechanical Properties of Solids

R. L. Cummerow, J. D. Venables

During the early part of this reporting period the following work was done to conclude our studies of MgO. Magnesium oxide had been selected for this work because it is obtainable as single crystals, because it is a typical ionic material with the simple NaCl structure, and because some techniques for studying its lattice defects and some of the properties of these defects were already known. No further work on this material is planned.

a. Creep of MgO. In earlier measurements of the creep of MgO single crystals the reproducibility of results was poor. It now appears that loading and unloading a sample during a series of tests to obtain its creep rate as a function of both load and temperature has a large effect on the creep behavior that is observed. Cooling and reheating a sample under constant load also affects its creep behavior. A standard procedure of maintaining a constant load on a specimen and heating it to successively higher temperatures for determinations of creep rate has been adopted and gives much improved results.

In creep tests three samples of MgO showed activation energies of about 4 ev while a fourth had a value of 7 ev. As mentioned in a previous report, MgO appears to creep at high temperatures by a dislocation-climb mechanism, which would be dependent upon self diffusion of cations and anions. The diffusion rate will depend upon the concentration of lattice vacancies, and for pure MgO this is only a function of temperature through an activation energy equal to half of the energy of formation of a magnesium-oxygen vacancy pair plus the energy of migration of a Mg^{++} vacancy. However, trivalent or tetravalent impurities in the MgO can require the formation of cationic vacancies to provide electrical neutrality, and this decreases the activation energy for creep. The ionic conductivity in alkali halides shows a similar decrease in

activation energy with the addition of divalent impurities. Such a hypothesis readily explains the occurrence of a high activation energy (7 ev) for a sample whose diffusion is controlled by the intrinsic properties of the MgO lattice and the lower activation energy (~4 ev) for samples in which the diffusion is extrinsically controlled by the impurities present. This discussion assumes that it is the diffusion of Mg^{++} rather than $O^{=}$ vacancies which is rate controlling. This is in accord with the higher activation energies reported for Mg self-diffusion (3.4 ev) than for O (2.7 ev).

It is known that the trivalent impurities iron and chromium, which occur in MgO crystals, can be reduced to divalent or lower by treatment in a reducing atmosphere. Figure G-2 shows the removal of a prominent band caused by ferric iron in the absorption spectrum of MgO by heating in a 15% H - 85% A atomosphere in a carbon tube furnace for one hour at 1960°C. However, this treatment did not cause any change in the activation energy for creep. Another sample was treated by passing an electric current through it at about 2000°C. Electrons are injected into the conduction band at the negative electrode. During their passage through the sample some of these electrons are trapped at trivalent (or possibly tetravalent) impurity levels in the forbidden gap, thus reducing these impurity ions. Figure G-3 shows that an untreated sample had an activation energy of essentially 4 ev while the treated sample showed an activation energy of about 7 ev. However, attempts to correlate this finding with spin-resonance determinations of the concentrations of trivalent chromium have not been successful. For both samples trivalent chromium is present to the extent of approximately 0.25 ppm. The trivalent iron content of these two samples has not yet been determined. However, from our previous experiment, where the trivalent iron was completely removed according to optical absorption, no effect on the creep behavior could be found. We are thus led to the tentative conclusion that the change in the creep behavior occasioned by the strong reduction, to which one sample of a pair was subjected, is not correlated with the amount of trivalent iron or trivalent chromium present. We thus believe that the 0.25 ppm trivalent chromium determined by spin resonance methods is too small to affect the creep rate in this temperature range and that some other tri- or tetravalent impurity is reducible by the electrical

method and is responsible for the change in creep behavior. Perhaps the impurity involved is not detectable by spin-resonance methods.

It will be noted that the extrinsic or 4 ev line in Figure G-3 will move up or down parallel to itself as the concentration or valence state of the controlling impurity is varied. Thus, we are furnished with a reasonable explanation for the great variation in creep rate among MgO samples. If we assume that the trivalent chromium content gives a lower limit for the intrinsic vacancy concentration at the lowest measurement temperature (1450°C), we can estimate the concentration of extrinsic vacancies present in the upper line by noting that the two lines cross at 1217°C. This concentration turns out to be 3.5 ppm. Thus, for this temperature range rather small concentrations of trivalent or tetravalent impurity are necessary to make profound changes in the creep rate.

b. Precipitation in MgO. Attempts were made during this period to diffuse various substances, such as Ca, Fe, etc., into single crystals of MgO to determine what element is responsible for the precipitate formation (that has been so much discussed in our earlier reports). The first material tried was CaO. The sample and powdered CaO were placed in a small pillbox consisting of a hollowed-out single crystal block of MgO. The pillbox was supported by a graphite substrate, heated in an argon atmosphere for 15 minutes at 2500°C in a 4" tube furnace, and allowed to furnace cool. Examination of the sample showed that the CaO had wet the MgO, but as far as could be determined, no diffusion or precipitation occurred. But while nothing of any interest took place in the sample, it was noted later that the pillbox contained a large number of precipitates in a region just inside the surface that had been in contact with the graphite support. Close examination in the optical microscope has shown that dislocations in this region, which extends about 45 μ below the surface, are heavily decorated with precipitate particles. Using dark-field illumination it is possible to see the decorated dislocations quite clearly. The precipitate takes the form of discrete particles spaced rather regularly along the dislocation, quite reminiscent of the precipitates observed in the electron microscope in as-grown MgO. It has been established that the particles form on single dislocations, dislocations in grain boundaries, and in what appear to be dislocation-free regions as well.

The experiment has been repeated several times since, and it has been found that, in addition to the precipitation of discrete small particles along dislocations, whiskers also grow inside the crystals. These whiskers may be seen by focussing below the surface of a treated sample with the optical microscope. It has been found that the whiskers are not attacked by the phosphoric-acid etchant used to polish MgO and are left behind on the surface of an etched sample. The whiskers generally grow in the direction of cube axes, both parallel and perpendicular to the treated surface. Thus, if an etched sample is tipped by 90° in the optical microscope so that the observer looks parallel to the treated surface, it is possible to see the whiskers sticking straight out of the MgO.

Since the whiskers are left behind on an etched surface, it was possible to strip them from the surface with a parlodian film and to obtain several electron micrographs and selected area diffraction patterns of the whiskers. The whiskers that were examined were about 0.5 μ wide and up to 0.2 mm long. The diffraction pattern revealed that the material is cubic and has exactly the same lattice constant (a_o = 5.16 Å) as the precipitated particles which have been under investigation in as-grown material. They, therefore, appear to be the same material, and this is consistent with the observation that neither the as-grown precipitates nor the whiskers are soluble in hot H_3PO_4. All work on MgO was terminated during this period.

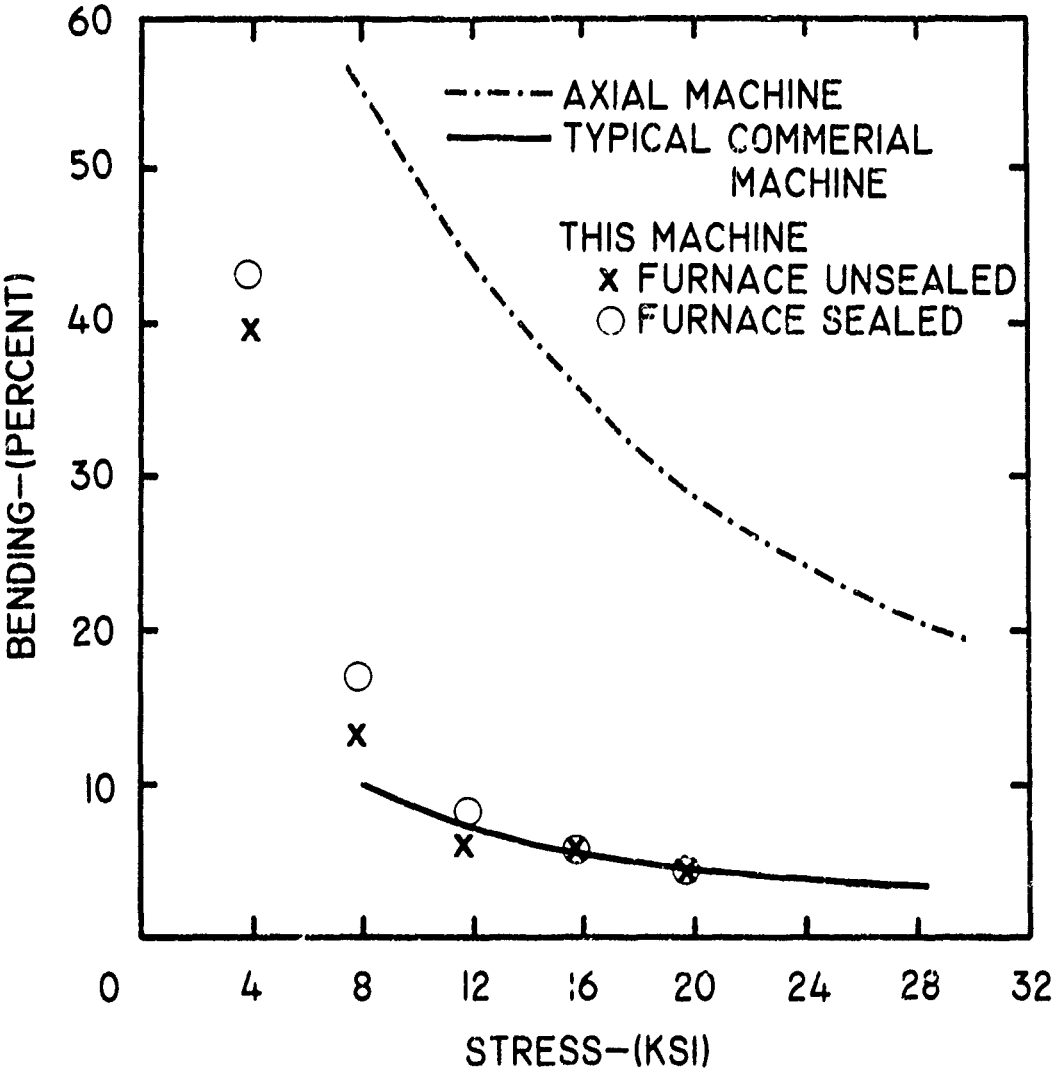

FIGURE G-1
COMPARISON OF ALIGNMENT

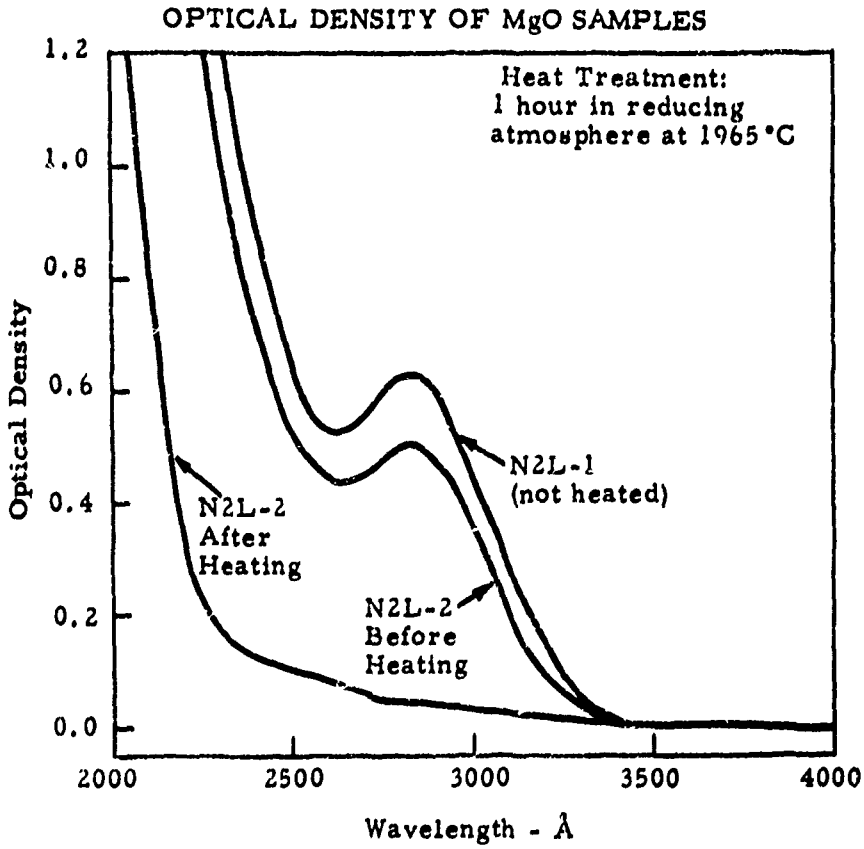
OPTICAL DENSITY OF MgO SAMPLES
Heat Treatment:
1 hour in reducing
atmosphere at 1965°C
Optical Density
1.2
1.0
0.8
0.6
0.4
0.2
0.0
N2L-1
(not heated)
N2L-2
After
Heating
N2L-2
Before
Heating
2000
2500
3000
3500
4000
Wavelength - Å

FIGURE G-2

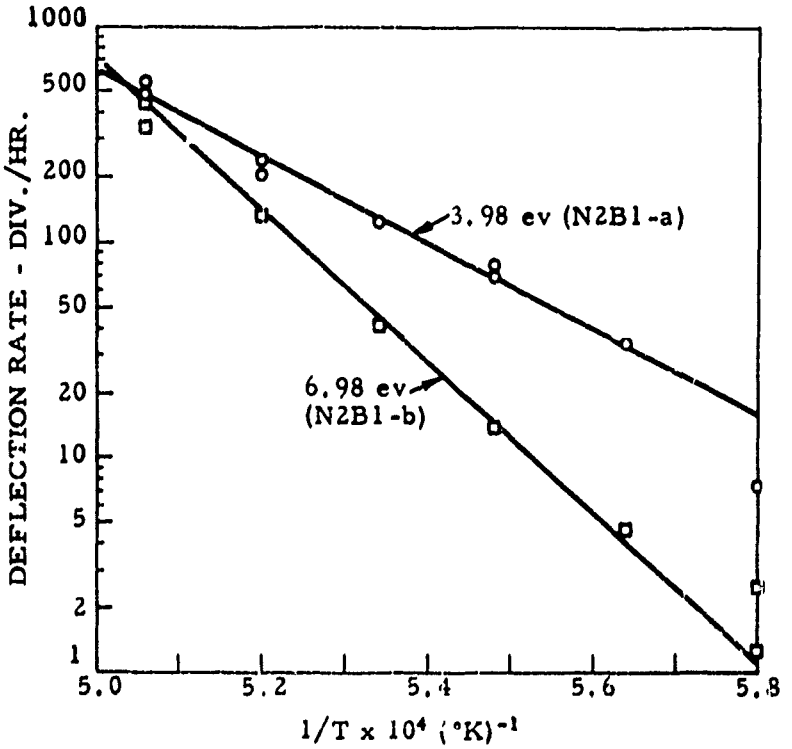
1000
500
200
100
50
20
10
5
2
1
DEFLECTION RATE - DIV./HR.
3.98 ev (N2B1-a)
6.98 ev
(N2B1-b)
5.0
5.2
5.4
5.6
5.8
1/T x 10⁴ (°K)⁻¹

FIGURE G-3

H. Thermal Properties

J. N. Pike

In the previous Semiannual Report, the results of measurements of the thermal conductivities of a series of GUF graphitized foams were reported. The success of a model in representing the results obtained was also cited. During the present period a series of measurements of the thermal conductivity of several samples of highly porous GPF graphitized foams have been made from 800° to 1900°C by the method of Powell and Schofield. The contribution, at high temperatures, of thermal radiation to the observed thermal conductivity can be described adequately by the pore model used previously in the analysis of data on GUF foams. The GPF foam has a smaller maximum pore size than the GUF foam, and so shows a smaller amount of radiative transport. The pore-wall parameters found by fitting the model to the data are consistent with the properties of poorly graphitized carbon for all foams measured.

All the information on both GPF and GUF foams is being incorporated in a report to be issued soon. Figure H-1 shows in summary the thermal conductivity values obtained for these foams of various porosities. Measurements were also made above 1900°C, but in this region the results were not reproducible because of physical and chemical changes in the graphite foams.

The report on the experimental details of the Rectangular Bar Method mentioned in the previous Semiannual Report has been issued. It is Research Report No. C-10, "High Temperature Thermal Conductivity Measurements Part II. The Rectangular Bar Method; Experimental Techniques" by J. N. Pike and J. F. Doar.

Work is now planned to measure the thermal and electrical conductivities and the specific heats of various refractory carbides and borides. Since the relatively long specimens required for the Rectangular Bar Method are difficult to fabricate, the rate of progress in measuring thermal properties of refractory carbides and borides will be governed largely by improvements in specimen preparation.

FIGURE H-I

COMPARISON OF MEASURED K'S OF TWO CLASSES OF GRAPHITIZED FOAM

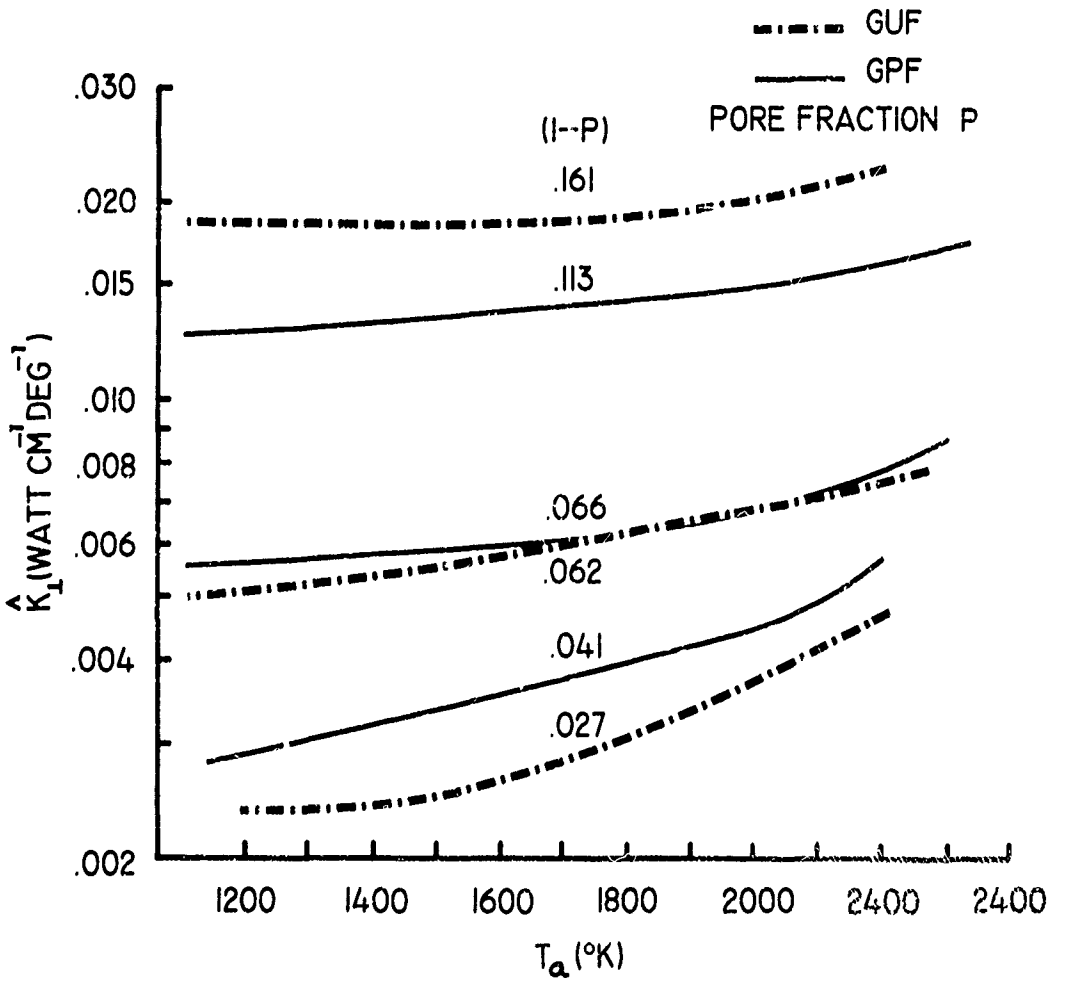

Advanced Research Projects Agency (6)
Washington 25, D. C.
Att: Advanced Propellant
Chemistry Office

National Aeronautics & Space (7)
Admin.
Washington 25, D. C.
Att: Office of Technical Information & Educational Programs
Code ETL

National Bureau of Standards
Washington 25, D. C.
Att: Dr. S. Madorskey

Att: Dr. Charles W. Beckett

Oregon Metallurgical Corporation
Albany, Oregon
Att: Mr. Russell G. Hardy

U.S. Atomic Energy Commission
Office of Technical Information Extension
Oak Ridge, Tennessee

U.S. Bureau of Mines
Pittsburgh 13, Pennsylvania
Att: M. P. Benoy, Reports Librarian, Explosives Research Lab.

Army Ballistic Missile Agency
Redstone Arsenal, Alabama
Att: ORDAB-HSI

Army Rocket & Guided Missile (4)
Agency
Redstone Arsenal, Alabama
Att: Technical Library
ORDXR-OTL

Att: ORDXR-OR

Att: ORDXR-IXD

Att: ORDXR-RFEP (12)

Army Rocket & Guided Missile Agency
Redstone Arsenal, Alabama
Att: Technical Library
ORDXR-RRH, Dr. T. A. Barr

New York Ordnance District, U.S. Army
New York 3, New York
Att: Facilities and Resources Branch

Att: ORDEH-O-TA

Office, Chief of Ordnance
Washington 25, D. C.
Att: ORDTB

Ordnance Office
Duke Station
Durham, North Carolina

Ordnance Materials Research Office
Watertown Arsenal
Watertown 72, Mass.

Dr. A. P. Levitt
Watertown Arsenal Laboratories
Watertown, Mass.

Aberdeen Proving Ground
Maryland
Att: Ballistic Research Lab.
ORDBG-BLT

Picatinny Arsenal
Dover, New Jersey
Att: Library

Diamond Ordnance Fuze Laboratories
Washington 25, D. C.
Att: ORDTL (012)

U.S. Naval Air Missile Test Center
Point Mugu, California
Att: Technical Library

U.S. Naval Ordnance Laboratory
Silver Spring, Maryland
Att: Library

U.S. Naval Ordnance Test Station
China Lake, California
Att: Technical Library Branch

U.S. Naval Propellant Plant
Indian Head, Maryland
Att: Technical Library

U.S. Naval Weapons Laboratory
Dahlgren, Virginia
Att: Technical Library

Office of Naval Research
Washington 25, D. C.
Att: Code 429

U.S. Naval Research Laboratory
Washington 20, D. C.
Att: Chemistry Div., Code 6130
R. R. Miller

Bureau of Naval Weapons
Washington 25, D. C.
Att: RMMP-2

Att: RMMP-4

Att: RMMP-331

Att: DLI-3 (2)

Att: RRRE-6

Special Projects Office
Department of the Navy
Washington 25, D. C.

Air Research & Development Center
Andrews AFB, Washington 25, D. C.
Att: RDRAPR

Air Force Flight Test Center
Edwards AFB, California
Att: FTR

Att: FTRP

Headquarters 6593rd Test Group
(Dev.)
Air Force Systems Command
Edwards AFB, California
Att: DGS

Air Proving Ground Center
Elgin Air Force Base, Florida
Att: PGAPI

Air Research and Development Command
Wright-Patterson AFB, Ohio
Att: WWRCPT-1

Headquarters, Space Systems Division
Air Force Systems Command
Los Angeles 45, California
Att: TDC

Aeronautical Systems Division
Wright-Patterson Air Force Base, Ohio
Att: ASRCNP

Armed Services Tech. Info. Agency (10)
Arlington 12, Va.
Att: TIPCR

British Defence Staff (4)
British Embassy
Washington, D. C.
Att: Scientific Information Center

Defence Research Member (4)
Canadian Joint Staff (W)
Washington 8, D. C.

Aerojet-General Corporation (3)
Sacramento, California
Att: Tech. Inf. Office

Aerojet-General Corporation
Azusa, California
Att: Library

Aeronutronic
Newport Beach, California
Att: L. H. Linder, Mgr.
Tech. Inf. Dept.

Aerospace Corporation (2)
Los Angeles 45, California
Att: Tech. Inf. Center
Acquisitions

Allied Chemical Corporation
Research Laboratory
Morristown, New Jersey
Att: H. R. Neumart

American Cyanamid Company
Stamford, Connecticut
Att: Dr. A. L. Pelker

Armour Research Foundation of
Illinois
Chicago 16, Illinois
Att: Fluid Dyn. and Prop.
Research, Dept. D

Atlantic Research Corporation
Alexandria, Virginia

Atomics International
Canoga Park, California
Att: Mr. J. Hove

Avco
Wilmington, Massachusetts
Att: Dr. E. Scalla

Att: Dr. H. L. Schick

Battelle Memorial Institute
Columbus 1 Ohio
Att: J. F. Lynch, Ceramics Div.

Att: C. S. Beaumont, DMIC

Borg-Warner Corporation
Kalamazoo, Michigan
Att: J. W. Schiffel, Chief
Engineer
Special Projects Dept.

The Carborundum Company
Niagara Falls, New York

Clevite Corporation
Cleveland 8, Ohio
Att: Mr. Gail Davies

Cornell Aeronautical Laboratories
Buffalo 21, New York
Att: Mr. J. Beale

Cornell University
Materials Science Center
Ithaca, New York
Att: Prof. R. L. Sproull

DeBell and Richardson, Inc.
Hazardville, Connecticut
Att: Mr. William Eakins

The Dow Chemical Company
Midland, Michigan
Att: Dr. R. S. Karpiuk, 1710 Bldg.

E. I. duPont deNemours and Company
Gibbstown, New Jersey
Att: Mrs. Alice R. Steward

Esso Research and Engineering Company
Linden, New Jersey
Att: Dr. J. P. Longwell

General Electric Company
Cincinnati 15, Ohio
Att: Tech. Info. Center

Georgia Institute of Technology
Mr. Cecil R. Mason, Ceramics Branch
Engineering Experiment Station
Atlanta, Georgia

The B. F. Goodrich Company
Research Center
Brecksville, Ohio
Att: Charles H. Stockman

Grand Central Rocket Company (3)
Redlands, California
Att: Helen Ashman, Librarian

Hercules Powder Company (2)
Allegany Ballistics Laboratory
Cumberland, Maryland
Att: Library

Hercules Powder Company
Rocky Hill Plant
Rocky Hill, New Jersey

Hercules Powder Company
Bacchus Works
Magna, Utah
Att: Librarian

Ionics, Inc.
Washington 5, D. C.
Att: Mr. S. G. McGriff
Asst. Director of Research

Jet Propulsion Laboratory
Pasadena 3, California
Att: I. E. Newlan, Chief
Reports Group

The Johns Hopkins University (3)
Solid Propellant Information
Agency
Applied Physics Laboratory
Silver Spring, Maryland

The Johns Hopkins University
Applied Physics Laboratory
Silver Spring, Maryland
Att: Dr. A. Westenberg

Prof. J. L. Margrave
University of Wisconsin
Madison 6, Wisconsin

Minnesota Mining and Manufactur- (2)
ing Company
St. Paul 6, Minnesota
Att: J. W. Millin

Northwestern University
Materials Research Center
Evanston, Illinois
Att: Prof. M. E. Fine

Olin Mathieson Chemical Corp. (3)
New Haven, Connecticut
Att: Miss Laura M. Kajuti

Olin Mathieson Chemical Corp.
Marion, Illinois
Att: Research Library

Rocketdyne (3)
Canoga Park, California
Att: Library 596-306

Rocketdyne
McGregor, Texas
Att: Library

Rocket Power
Pasadena, California
Att: Dr. Milton Farber, Vice Pres.

Shell Development Company
Emeryville 8, California

Space Technology Laboratory, Inc.
Los Angeles 45, California
Att: Mr. Robert C. Anderson

Thiokol Chemical Corporation
Huntsville, Alabama
Att: Technical Director

Thiokol Chemical Corporation
Elkton, Maryland
Att: Librarian

Thiokol Chemical Corporation (2)
Brigham City, Utah
Att: Library Section

Thiokol Chemical Corporation
Rockets Operation Center
Ogden, Utah
Att: Librarian

United Technology Department
Sunnyvale, California
Att: Librarian

University of Pennsylvania
Laboratory for Research on Structure
of Matter
Philadelphia 4, Pennsylvania
Att: Prof. J. N. Hobstetter

Wright Aeronautical Corporation (2)
Wood-Ridge, New Jersey

Aeronautical Systems Division (2)
Wright-Patterson AFB, Ohio
Attn: Mr. W. G. Ramke
Code: ASRCMC

Alpha Research & Development, Inc. (2)
Blue Island, Illinois
Att: Dr. Robert Patrick

UNION CARBIDE CORPORATION:

Dr. J. C. Bowman
Mr. E. J. Boyle
Dr. R. G. Breckenridge
Dr. R. M. Bushong
Dr. R. L. Cummerow
Mr. H. A. Downey
Dr. D. M. Gillies
Mr. D. E. Hamby
Dr. A. B. Kinzel
Dr. R. A. Charpie
Helen F. Kuhns, Librarian,
Haynes Stellite Company
Dr. R. W. McNamee
Mr. R. M. Milton
Dr. John Pike
Dr. P. O. Schissel
Dr. Milton Stern
Mr. W. A. Steiner
Dr. Roy C. Sundeen
Mr. J. D. Venables
Mr. G. H. Wagner
Mr. H. L. Willard